

1 **Thresholds for estuarine compound flooding using a combined** 2 **hydrodynamic-statistical modelling approach**

3 Charlotte Lyddon¹, Nguyen Chien², Grigorios Vasilopoulos³, Michael Ridgill⁴, Sogol Moradian⁵,
4 Agnieszka Olbert⁵, Thomas Coulthard⁵, Andrew Barkwith⁶, Peter Robins⁴

5
6 ¹Department of Geography and Planning, University of Liverpool, UK

7 ²School of Engineering, Edinburgh University, UK

8 ³School of Environmental Sciences, University of Hull, Hull, England, UK

9 ⁴School of Ocean Science, Bangor University, UK

10 ⁵Civil Engineering, University of Galway, Ireland

11 ⁶British Geological Survey, Keyworth, Nottingham, UK

12 *Correspondence to:* Charlotte Lyddon (c.e.lyddon@liverpool.ac.uk)

13 **Abstract.** Estuarine compound flooding can happen when an extreme sea level and river discharge occur concurrently, or in
14 close succession, inundating low-lying coastal regions. Such events are hard to predict and amplify the hazard. Recent UK
15 storms, including Storm Desmond (2015) and Ciara (2020), have highlighted the vulnerability of mountainous Atlantic-facing
16 catchments to the impacts of compound flooding including risk to life and short- and long-term socioeconomic damages. To
17 improve prediction and early-warning of compound flooding, combined sea and river thresholds need to be established. In this
18 study, observational data and numerical modelling were used to reconstruct the historic flood record of an estuary particularly
19 vulnerable to compound flooding (Conwy, North-Wales). The record was used to develop a method for identifying combined
20 sea level and river discharge thresholds for flooding using idealised simulations and joint-probability analyses. The results
21 show how flooding extent responds to increasing total water level and river discharge, with notable amplification **in flood**
22 **extent** due to the compounding drivers in some circumstances, and sensitivity (~7%) due to **the-a 3-hour** time-lag between the
23 drivers. The influence of storm surge magnitude (as a component of total water level) on flooding extent was only important
24 for scenarios with minor flooding. There was variability as to when and where compound flooding occurred; most likely under
25 moderate sea and river conditions (e.g. 60-70th and 30-50th percentiles), and only in the mid-estuary zone. For such cases, joint
26 probability analysis is important for establishing compound flood risk behaviour. Elsewhere in the estuary, either sea state
27 **(lower-estuary)** or river flow **(upper-estuary)** dominated the hazard, and single value probability analysis is sufficient. These
28 methods can be applied to estuaries worldwide to identify site-specific thresholds for flooding to support emergency response
29 and long-term coastal management plans.

30 **1 Introduction**

31 Estuaries are the most dynamic coastal systems – crucial for global water and nutrient cycling, biodiversity of natural habitats,
32 and provide ecosystem services such as food security and tourism that shape the livelihoods and well-being of their
33 communities (Barbier et al., 2011). They hold strategic value for world trade, supporting haulage and fisheries, with significant
34 growth opportunities, e.g., in marine energy. About 60% of the world’s population lives along coastal and estuarine zones
35 (Lindeboom et al., 2020) and 36% of the UK lives within 5 km of the coast (Census, 2020). Each year people make over 270
36 million recreational visits to UK coasts (Elliott et al., 2018) and generate £17.1 billion in tourist spend (NCTA, 2023). Sea-
37 level rise and changing storm patterns, along with intensification of human activity in and around estuaries, e.g., littoralisation,
38 farming, and water management, means estuarine communities are increasingly vulnerable to the impacts of extreme events –
39 of which in the UK flood hazards are rated as the second highest risk for civil emergencies, after pandemic influenza, (HM
40 Government, 2020; EA, 2023).

41

42 Estuaries are at the interface of marine (tide, storm surges, waves), hydrological and terrestrial (precipitation causing river
43 discharge, runoff, snow melt, groundwater) physical processes, which interact over a range of temporal and spatial scales
44 (Chilton et al., 2021). [Standard terms follow the definitions outlined in Pugh \(1987\) and Chow et al. \(1988\).](#) Flooding can
45 occur when one or several of these processes cause water levels to exceed a critical threshold, such as a sea defence (EA,
46 2022). [A threshold represents a meteorological, river and/or coastal condition at which flooding hazard increases \(Sene, 2008\).](#)
47 [If a forecasted storm event could exceed the threshold then action to mitigate the hazard should be taken, for example, issue a](#)
48 [flood warning.](#) In the UK, coastal flooding has an annual cost of up to £2.2 billion for flood management and emergency
49 response (Penning-Rowell, 2015). Estuaries are particularly vulnerable to the effects of compound flood events when coastal
50 and fluvial drivers can occur concurrently or in close succession [to generate flooding](#) (Svensson and Jones, 2004; Couasnon,
51 et al., 2020; Bevacqua et al., 2020; Robins et al., 2021). High sea-levels can occur due to astronomical high spring tides and
52 can be further exacerbated when they co-occur with storms generating large surges and waves at the coast. Alongside this,
53 storms can generate heavy precipitation and lead to high fluvial and pluvial flows, which increases flood hazards within
54 estuaries (Ward et al., 2018). A compound event caused devastating flood impacts in Lancaster, [NW-England](#) following Storm
55 Desmond, 4–6 December 2015, due to extended heavy rainfall and river discharges coinciding with an incoming tide (Ferranti
56 et al., 2015).

57

58 Statistical analyses of long-term data, e.g., from paired coastal and riverine gauge observations can show dependence between
59 these drivers (Hendry et al., 2019; Camus et al., 2021; Lyddon et al., 2022) and can be used to examine the joint exceedance
60 probability of estuary water levels based on when marine and terrestrial drivers are above the predefined thresholds (e.g., 95th
61 or 99th percentile) (Kew et al., 2013, Salvadori et al., 2016). Estuaries on the west coast of Britain are more likely to experience
62 co-dependent extreme events and compound flooding than those on the east coast, due to the prevailing southwesterly storm

63 tracks that can bring extreme storm surges and concomitant rainfall – the generally short and mountainous west coast
64 catchments causing river flows to increase quickly and coincide with the surge (Haigh et al., 2016). Beyond the floods in
65 Lancaster, [NW-England](#), Storm Desmond caused severe compound flooding across several estuaries of west and southwest
66 Britain, amounting to over £500m in flood-related damages (Bilskie and Hagen, 2018; Matthews et al., 2018). Flooding in
67 estuaries on the east coast of Britain is more likely to be driven by independent surge and rainfall events because the catchments
68 tend to be larger with slower runoff times and easterly storms tend not to be coupled with heavy rainfall (Svensson and Jones
69 2002), although the generally longer durations of high river flows (e.g., several days for the Humber, [NE-England](#)) increases
70 the chances of high discharge coinciding with high sea levels from a separate storm. Modelling studies have shown the
71 likelihood and impacts of compound flooding at local (Robins et al., 2021) and national scales (Ganguli and Merz, 2019;
72 Eilander et al., 2020; Feng et al., 2023; Eilander et al., 2023), but do not specify driver thresholds that lead to compound
73 flooding and spatial variability in flooding of different driver combinations.

74
75 Defining critical driver thresholds for estuary flooding is crucial for the early detection and forecasting of flood events to issue
76 timely warnings, for operational purposes such as emergency response, and for identifying vulnerable areas to focus
77 intervention and coastal management strategies (EA, 2009). Early warning systems and appropriate planning measures are the
78 most widely used and reliable tools to ensure community preparedness (Alfieri et al., 2012). Early warning systems and
79 subsequent responses require a thorough understanding of hazard behaviour and classification, and knowing when a specific
80 environmental condition will be passed to cause flooding is vital in this framework (Šakić Trogrlić et al., 2022). Terrestrial-
81 driven floods and marine-driven floods are generally considered separately in operational flood risk assessments (e.g.
82 CoSMoS, USA (USGS)), and there is currently a UK government policy gap in terms of estuary flood risk (EA, *pers. comm.*).
83 Flood assessments show when a critical threshold is exceeded to cause either fluvial or coastal flooding, but do not consider
84 compound events. Modelling statistical and probabilistic methods can contribute to an understanding of the unique response
85 of each estuary to flood drivers, where catchment typology, tidal regime, and estuary characteristics influence the behaviour
86 of the hazard. The same water level return period at a location within an estuary can be caused by different drivers and cause
87 different flood extents, showing the importance of understanding a range of site-specific, compound event scenarios alongside
88 their joint probability (Olbert et al., 2023).

89
90 This research aims to identify the coastal and fluvial conditions that lead to flooding in an estuarine system. The research will
91 use a combination of historic records of flooding, instrumental data, statistical analyses, and numerical modelling tools to
92 identify the combined driver thresholds which cause flooding, and which areas within the estuary are vulnerable to the
93 compounding effects. The research is applied to the Conwy Estuary, [North Wales \(N-Wales\)](#) as an example of a mountainous,
94 flashy catchment on the west coast of Britain which is vulnerable to the effects of storm-driven, compound flooding. The case
95 study and methodology are described in section 2, which demonstrates how historic records of flooding are supplemented with
96 online sources, instrumental data from a paired river and tide gauge, and results from an inundation model (section 3). Joint

97 probabilities are assigned to coastal and fluvial conditions before results are considered in the context of wider flood hazard
98 policy to improve the accuracy of flood records and flood hazard assessments in the context of future climate change and land
99 use change for improved resilience of coastal communities (section 4).

100 2 Methods

101 2.1 Conwy Estuary, North Wales

102 The Conwy Estuary is a steep and mountainous catchment in ~~North-N~~-Wales that has been shown to be one of the most
103 vulnerable in Britain to compound events of extreme surges coinciding with extreme river flows (Lyddon et al., 2021). The
104 estuary is macrotidal, which is common for the UK, with a 4-6 m tidal range. The semi-diurnal tide displays pronounced tidal
105 asymmetry, characterised by short, fast flood tides and longer, slower ebb tides, which is typical of many macrotidal estuaries.
106 Current speeds reach 1.3 m s⁻¹ during the 2.75 hr flood, while ebb current speeds are 25-30% smaller (Jago et al., 2023). The
107 estuary is subject to the effects of surge generating, low pressure Atlantic storms, elevating sea level up to 1.6 m above
108 predicted levels. The towns of Llanrwst in the upper estuary, and Conwy and Llandudno in the lower estuary are vulnerable
109 to this hazard, and communities, businesses, and transport networks are affected by several floods each year. Most notably,
110 the primary road and rail network connecting north and south Wales runs through the Conwy Valley. Storm Ciara, 9 February
111 2020, exemplifies the complexities of compound flooding. Ciara atypically came from the north bringing intense rainfall (80
112 mm in 15 hrs) that inundated the estuary floodplains to capacity and held back by the rising spring tide plus 0.72 m surge.
113 Record-breaking flows (529 m³/s) in the main river ensued, causing widespread flooding (> 150 properties) and a ‘backwater
114 effect’ that flooded transport links and caused power outages. There was no warning, so residents and landowners had no
115 chance of activating safety measures. Flooding was recorded throughout the community in local and regional news outlets
116 (BBC, 2020; Evans, 2020; Spridgeon, 2020).

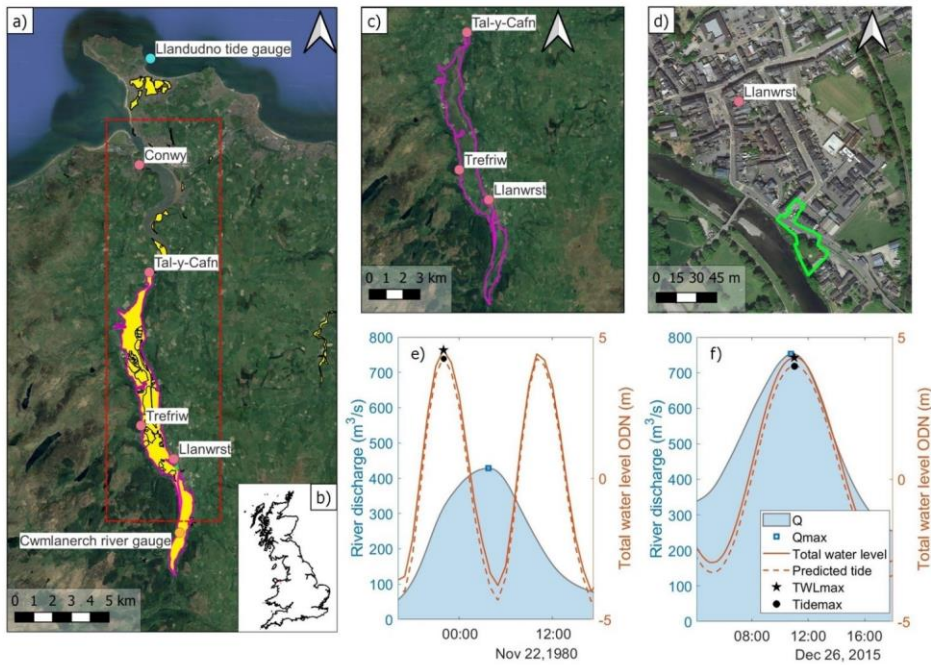
117
118 The Conwy Estuary has a record of instrumental, observation data available from the Cwmlanerch river gauge
119 (<https://nrfa.ceh.ac.uk/data/station/info/66011>) and Llandudno tide gauge (<https://ntsif.org/tgi/portinfo?port=Llandudno>).
120 River discharge recorded at Cwmlanerch is available at a 15-minute temporal resolution from November 1980-February 2023,
121 with 99% data coverage in time. The total water level recorded at Llandudno is available at a 15-minute temporal resolution
122 from January 1994-December 2020, with 88% data coverage in time. Total water level from the Llandudno tide gauge was
123 linearly detrended to remove the effects of a historical sea level trend from the time series (Coles 2001). Historic records of
124 flooding extend back to the 1980’s before the instrumental tide gauge data began, therefore tide and surge reanalysis data for
125 this period were obtained from the Global Tide Surge Model (GTSM). The third-generation GTSM (Kernkamp et al., 2011)
126 has a coastal resolution of 1.25 km within Europe and is forced with meteorological fields from the ERA5 climate reanalysis
127 to simulate extreme sea levels for the period 1979 to 2017. The tide and surge model has shown good agreement between

128 modelled and observed sea-levels, and is applicable to flood risk and climate change research (Muis et al., 2016; Muis et al.,
129 2020; Wang et al., 2022). The record length used in the analysis here is determined by the monitoring and modelling duration.

130 2.2 Historic records of flooding in Conwy

131 Natural Resource Wales (NRW) has collated information on Recorded Flood Extents to show areas that have flooded in the
132 past from rivers, the sea or surface water, which is documented on an open-source, online data catalogue (NRW, 2020). The
133 database of polygons (Figure 1a) shows 22 Recorded Flood Extents in the tidally-influenced Conwy estuary. Of these Recorded
134 Flood Extents, 14 events Incidences of flooding were driven by high sea levels or river flows or both that caused flooding by
135 channel capacity exceedance or overtopping of defences (i.e., ignoring flooding due to obstructions, blockages, local drainage
136 issues, and excess surface water was ignored). This left 14 records of flooding caused by channel capacity exceedance or
137 overtopping of defences, but Instrumental river gauge data is was only available for six of these 14 events. The behaviour of
138 the drivers of the six Recorded Flood Events was identified-reconstructed from the sea level and river flow data records,
139 including timing and magnitude of peak river discharge (Q_{max}), total water level (TWL_{max}), predicted tide level, and skew
140 surge that preceded the flood (e.g., Figures 1e and 1f). Figures 1c and 1e show the 22 November 1980 compound event where
141 Q_{max} was recorded as 428 m³/s at 03:45 am, and TWL_{max} was 4.5 m at 22:00 am (which included a 0.25 m skew
142 surge) however lack of exact information on the timing of the flooding makes it difficult to determine if TWL_{max} contributed
143 to flooding, and whether this was a compound flood. The NRW catalogue notes that there was widespread flooding in the
144 Conwy Valley at this time, although since this was the pre-internet era there are no further online records. Figures 1d and 1f
145 show the 26 December 2015 compound event where Q_{max} was recorded as 753 m³/s at 10:45 am, and TWL_{max} was 4.3 m at
146 11:00 am (which included a 0.3 m storm surge). The short, 15-minute time lag between Q_{max} and TWL_{max} , and extreme
147 magnitudes (Q_{max} was an 85th percentile event and TWL_{max} was an 84th percentile event), caused extensive flooding in
148 Llanwrst and across the valley (ITV, 2015; Welsh Government, 2015; Jones, 2016; NRW, 2016); however, the Recorded Flood
149 Event in the NRW catalogue covers only a small area at Llanwrst (Figure 1d). This suggests that historic records of flooding
150 in the Conwy are incomplete, hence there is a need for further information on the drivers and impacts of flooding from which
151 to establish flood prediction patterns and thresholds. Natural Resource Wales NRW identifies that the absence of a Recorded
152 Flood Extent does not mean the area has not flooded. This information gap is expected throughout the UK.

153



154

155

156 **Figure 1: (a-b) Location and extent of all Recorded Flood Events (yellow shading) in the region of interest (red dashed**

157 **box) in the Conwy Estuary, N-Wales. The outlines of two Recorded Flood Events are highlighted; 21 November 1980**

158 **(pink polygon) and 26 December 2015 (green polygon), which are shown in more detail in (c) and (d). (e-f) Time series**

159 **of river discharge, total water level and predicted tide for two Recorded Flood Events in (c) and (d). [Figure 1a-c](#)**

160 **[Basemap © OpenStreetMap 2023](#)**

161

162 Flood drivers Q_{max} and TWL_{max} during the six Recorded Flood Events in NRW's data catalogue are shown as stars in Figure

163 2. Additionally, [from analysis of the ~40 years of river/sea gauge data \(see Section 2.1\)](#), the top 50 most extreme Q_{max} and

164 corresponding TWL_{max} events within a 'storm-window' are shown as circles in Figure 2 [\(each of these corresponding events](#)

165 [occur within a 'storm-window' of one another, defined as 20.25 hours for the Conwy based on the average duration of extreme](#)

166 [event hydrographs over a 30-year period; Lyddon et al., 2021\)](#) (where the storm-window was defined as 20.25 hours for the

167 [Conwy based on the average duration of event hydrographs over a 30-year period; Lyddon et al., 2021\)](#). Gaps in the tide gauge

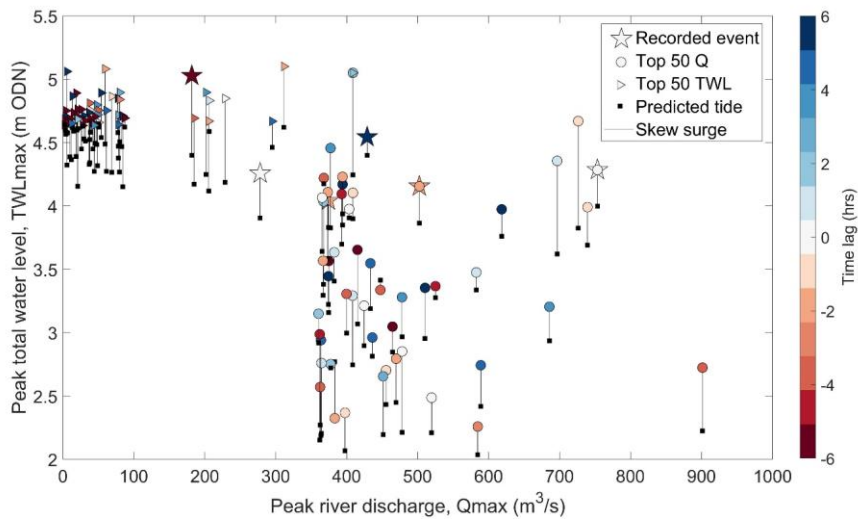
168 record meant that in effect the top 72 Q_{max} events were selected, to identify 50 events paired with TWL_{max} . Similarly, the
169 top 50 most extreme TWL_{max} and corresponding Q_{max} events are shown as triangles in Figure 2. For all paired events plotted,
170 the time lag in hours between Q_{max} and TWL_{max} is represented by the shape colour, and the vertical black line indicates the
171 magnitude of the skew surge. One top 50 Q_{max} event corresponded with a top 50 TWL_{max} event, so that 99 extreme events
172 were identified. Not all of these 99 extreme events from the gauge records necessarily caused flooding but this data highlights
173 that there are potentially many events that caused flooding that are not recorded, as explored below. Further, two of the six
174 Recorded Flood Extents corresponded with the 99 extreme events, meaning a total of 103 events are plotted in Figure 2.

175
176 The recorded most extreme Q_{max} was 901.31 m³/s, which occurred on 16 March 2019, and coincided with a TWL_{max} of 6.57
177 m (a neap tide reaching 6.08 m combined with a 0.49 m skew surge), where there was a time lag of +3½ hrs (i.e., Q_{max}
178 occurred on the ebbing tide). The relatively long time lag and less extreme TWL_{max} means that this was predominantly a
179 fluvial-driven event, rather than a compound event. Flooding was recorded across the UK including in the Conwy on this date
180 following a particularly wet period that included two major storms, Freyer and Gareth (Met Office, 2019). The recorded most
181 extreme TWL_{max} was 8.95 m (a spring tide of 8.47 m with a skew surge of 0.48 m), which occurred on 10 February 1997, and
182 coincided with a Q_{max} of 311.52 m³/s, where there was a +1½ hour time lag (again Q_{max} occurred on the ebbing tide). Whilst
183 coastal flooding was recorded in the Conwy Tidal Flood Risk Assessment (HRW, 2008), there was no flooding recorded within
184 the estuary so it is not considered as a compound event.

185
186 Of the top 50 Q_{max} events, 39 had a time lag of ± 2 hours or less, of which 14 events had a time lag of ± 1 hour or less,
187 showing that concurrence of Q_{max} and TWL_{max} has occurred regularly in the past. Although there was only one occasion
188 when a top 50 Q_{max} and top 50 TWL_{max} co-occurred, and this event had a time lag of about an hour. Seven of the top 50
189 TWL_{max} events had a time lag of ± 2 hours or less, of which two events had a time lag of +1 hour or less. It is also worth
190 noting that all top 50 TWL_{max} events occurred around midday (10:30–12:15) or midnight (22:45–00:00). Spring high tides
191 are phase-locked around midday and midnight for the Conwy region, hence increasing the chances of an extreme water level
192 at these times.

193
194 Three standout events are circled in Figure 2 which could be interpreted as compound events, all with extreme river discharges
195 ($Q_{max} > 700$ m³/s and $> 77^{\text{th}}$ percentile), high total water levels ($TWL_{max} > 4$ m and $> 84^{\text{th}}$ percentile), and time lags under
196 ± 1 hour. One of these three events is starred as a Recorded Flood Event on the NRW data catalogue (26 December 2015);
197 however, the others are not. It is important to know whether all of these extreme events in fact caused flooding as one might
198 expect, and which other extreme events in the ~40 year record led to flooding, to be able to establish meaningful thresholds
199 for flood warning.

200



201

202

203 **Figure 2: Recorded Flood Events-Extents at Conwy (stars), top 50 Q_{max} events at Cwmlanerch (circles), top 50**
 204 **TWL_{max} events at Llandudno (triangles), and associated predicted tide (black square) and skew surge magnitude**
 205 **(vertical black line) for each event. Colours indicate the length of time lag between peaks in river discharge and total**
 206 **water level (negative time lags indicate that Q_{max} arrived before TWL_{max} and so coincided with a flooding tide).**

Formatted: Font: Italic

Formatted: Font: Italic

207 **2.3 Extending the record of flooding**

208 Records of historic flood events were expanded by exploring internet records. Online resources were used to identify if flooding
 209 happened as a result of extreme coastal and/or river conditions to create a more comprehensive record of historic flood events.

210 Web scraping approaches (also referred to as web extraction or web harvesting) were used to evaluate whether there is further
 211 evidence of recorded flooding in the Conwy estuary within the 100-99 extreme Q_{max} and TWL_{max} events plotted in Figure 2.

212 The dates of all recorded extreme events were searched on DuckDuckGo, Microsoft Bing, and Google. No evidence of flooding
 213 was available for events prior to 1990; online records prior to this date are unreliable and before the 'internet era'.

214 Predetermined searches specified any evidence must be for an event in the Conwy Estuary from Deganwy upstream to Llanrwst
 215 (i.e. the dashed box in Figure 1a). Train and bus cancellations were also considered evidence of flooding events. A railway

216 line runs between Deganwy and Llanrwst, stopping at Llandudno Junction, Glan Conwy, Tal-y-Cafn and Dolgarrog, so these
 217 stations were included in the web search. Results were supplied in browser tabs for analysis. If a date was deemed a 'flooding

Formatted: Font: Italic

Formatted: Font: Italic

218 event', the supporting evidence was investigated to see if there was any information to note the drivers of the flooding (Table
219 1).

220 *Table 1: Description of labels used to assign a cause of flood tag to a date*

221

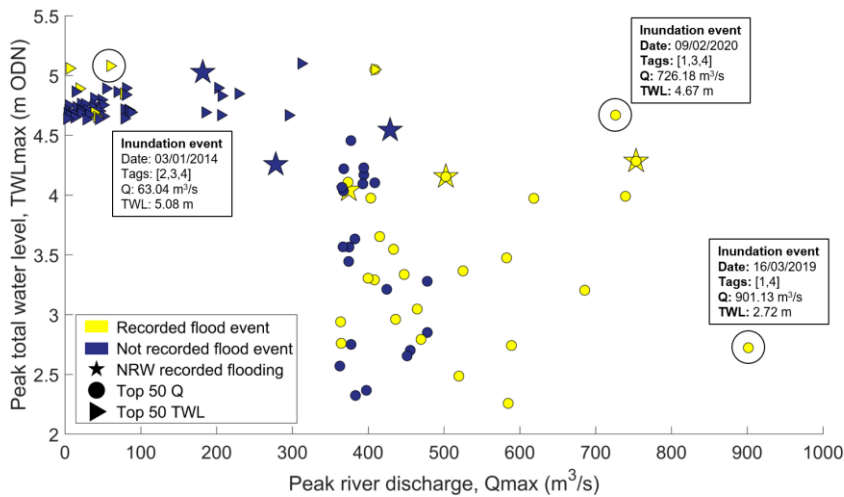
Label	Code
0	None
1	River discharge
2	Storm surge
3	High tide
4	Storminess

222

223

224 The web searches isolated an additional 26 recorded floods ~~that matched extreme events in our analysis~~, as shown in Figure 3,
225 with yellow ~~dots-circles~~ indicating ~~these 26 events, there is evidence of flooding and~~ The blue ~~dots-circles in Figure 3 indicating~~
226 ~~indicate extreme events where there was no online evidence there is no evidence~~ of flooding. Labels assigned to three of the
227 inundation events are shown in the figure. Multiple sources of evidence indicate a marine-driven flooding event on 3 January
228 2014, largely due to an extreme storm surge of 0.8 m, including railway cancellations, home evacuations, and road closures
229 (Welsh Government, 2014; Sibley et al., 2015). Evidence of river-driven flooding on 16 March 2019, during Storm Gareth,
230 was derived from news reports of damage to over 40 homes, road closures, and flood warnings issued by NRW (BBC, 2019;
231 FloodList, 2019; Met Office, 2019). Evidence of river-driven and marine-driven flooding suggests that 9 February 2020 was
232 a compound flood event. Figure 3 provides a more comprehensive record of flood inundation than shown in Figure 2; however,
233 data gaps in instrumental time series, online evidence, and what information was recorded, leave uncertainty in where to set
234 driver thresholds and patterns for flooding, especially for less extreme Q_{max} and TWL_{max} that led to compound flooding.

235



236
 237 **Figure 3: Recorded flood extents, and top 50 Q_{max} and top 50 TWL_{max} events, colour coded to show those events**
 238 **which are were inundation events (yellow) and those which are were non-inundation events (blue). Three events**
 239 **highlighted to show drivers, timing, and labels for the cause of flooding.**

Formatted: Font: Italic

Formatted: Font: Italic

240 2.4 Hydrodynamic inundation model

241 The Caesar-Lisflood hydrodynamic model (Coulthard et al., 2013; Skinner et al., 2015; Harrison et al., 2022) was used within
 242 a sensitivity test framework to simulate a series of idealised event scenarios which represent plausible combined river and sea
 243 level conditions, to identify which combination of drivers leads to flooding in the Conwy. CAESAR-Lisflood is a
 244 geomorphological and landscape evolution model that combines the Lisflood-FP 2D hydrodynamic flow model (Bates et al.
 245 2010) with the CAESAR geomorphic model. Lisflood uses a flow routing algorithm that determines the direction of flow
 246 based on the elevation gradient, and conserves mass and partial momentum. CAESAR-Lisflood does not run in 3D, and this
 247 functionality is not required to explore flood inundation. Baroclinicity is not an important process to represent for this research,
 248 and would require additional computational expense.

249 2.4.1 Model domain

250 The model domain includes the tidally influenced Conwy estuary, downstream of the Cwmlanerch river gauge on the River
 251 Conwy and extending offshore into Conwy Bay and the Menai Strait at the coastal boundary. A number of sources were
 252 combined to generate the land elevation data required to build the model, including (a) seabed bathymetry, (b) land elevations

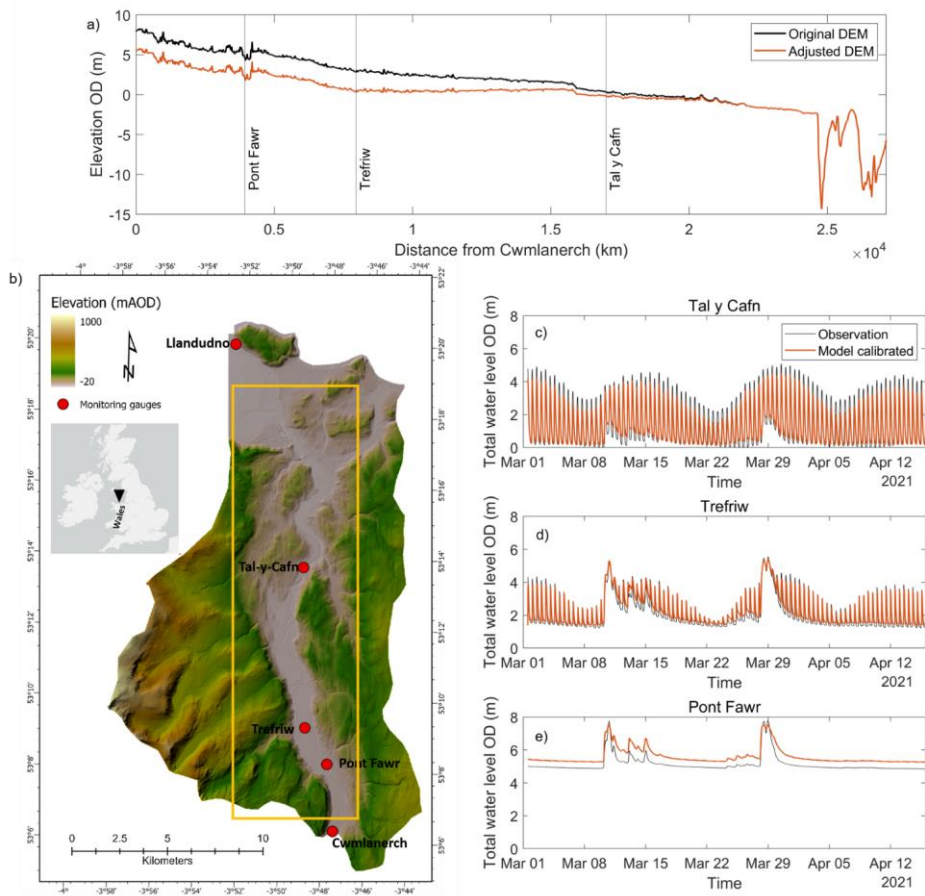
253 and (c) location and heights of existing flood defences. The domain topography was based on the marine DEM, Lidar DTM
254 and OS Terrain 5m DTM, [all available through Digimap \(https://digimap.edina.ac.uk/\)](https://digimap.edina.ac.uk/). The Lidar DTM data was used to check
255 and, where necessary, augment the flood defences vector database, [n obtained from the NRW data catalogue](https://datamap.gov.wales/)
256 [\(https://datamap.gov.wales/\)](https://datamap.gov.wales/). The processing steps undertaken to produce the model domain are described in Supplementary
257 Information S1.

258 2.4.2 DEM calibration

259 Caesar-Lisflood was run in reach mode, in which the model is forced with discharge and water level time series at the upstream
260 (river) and downstream (offshore) boundaries, respectively. For the upstream boundary, a time series of water discharge (m^3/s)
261 measured at the Cwmlanerch gauge was used. The dataset provided by NRW has a 15-minute temporal resolution and covers
262 the calibration period: 1 March-16 April 2021. For the offshore boundary, a time series of measured sea levels at Llandudno
263 was used, provided by the British Oceanographic Data Centre (BODC). It contains measured levels above the Llandudno Chart
264 Datum (CD) at 15-minute intervals and spans the same period as the time series of discharge. The tidal water levels were
265 converted to Ordnance Datum (OD) by adjusting for the vertical offset between CD and OD (i.e. -3.85 m). The Manning's
266 roughness coefficient for the river channels and marine areas was set to 0.022, the Courant number at 0.6 and the Froude limit
267 at 0.8. To avoid water accumulation behind flood defences when overtopping occurred, a water loss function of 0.2 m day^{-1}
268 was applied. The function was only applied to the floodplains to avoid affecting river or sea water levels. Only the
269 hydrodynamic component of the model was used for the simulations described here and simulated water levels were exported
270 at 15-minute intervals for further analysis.

271
272 Simulated water levels were compared against corresponding values obtained from gauges within the estuary at Pont Fawr,
273 Trefriw and Tal-y-Cafn (see Figure 4). The gauges at Pont Fawr and Trefriw are maintained by NRW and monitor water levels
274 at 15-minute intervals, relative to OD. At Tal-y-Cafn a pressure logger was installed in October 2020 (Lat. 53.23°N , Lon.
275 3.82°W) that also provided measured water levels, relative to OD at 15-minute intervals. Initially the DEM had incorrect
276 channel bed elevations due to the LiDAR shortcomings for inundated areas (further detail in S1). [We approximated the correct](#)
277 [channel bathymetry by manually adjusting the channel bed elevations, re-running the simulation and comparing simulated and](#)
278 [observed water levels. We repeated this process until we reached a satisfactory agreement between observed water levels and](#)
279 [model predictions at the three gauges. With this method the bed profile is adjusted until it simulates the observed water profile](#)
280 [taking into account flow non-uniformity \(Neal et al., 2022\). Therefore, we followed the concept described by \(Neal et al.,](#)
281 [2022\) of using channel bathymetry as a calibration parameter. Indeed we gradually adjusted the channel bed elevations and](#)
282 [ran the simulation in a stepwise manner until we reached a satisfactory agreement between simulated and observed water](#)
283 [levels.](#) The calibrated DEM is shown in Figure 4a together with the locations of the various gauges used in the study. After the
284 final DEM adjustment (Figure 4b), RMSE values were 0.59 m, 0.39 m, and 0.69 m (Figure 4c-e) [and the Kling-Gupta](#)
285 [Efficiency \(Gupta et al., 2009\) values were 0.90, 0.90 and 0.70](#) for Pont Fawr, Trefriw and Tal-y-Cafn, respectively. Flood

286 peaks were isolated in the calibration period and RMSE values were 0.57 m, 0.19 m, and 0.29 m for Pont Fawr, Trefriw and
287 Tal-y-Cafn. Improved RMSE scores for flood peaks indicates the model is able to capture the magnitude of the largest and
288 most prominent peaks. ~~Higher RMSE and weaker KGE in the upper estuary could be attributed to the lack of tributaries in the~~
289 ~~model, but the set up remains suitable for the purposes of this research.~~ Higher RMSE values in the upper estuary (Pont Fawr
290 gauge) could be attributed to the omission of tributaries in the model that flow into the Conwy downstream of the Cwmlanerch
291 gauge (upstream boundary of the model). These inputs are, as a result, not represented in the discharge data forcing the model.
292 Nevertheless the set up remains suitable for the purposes of this research



293

294 **Figure 4 a) Calibrated Conwy estuary model domain showing elevations relative to Ordnance Datum and location of**
 295 **monitoring gauges. The region of interest in the estuary is shown (orange box, size 3920 × 19580 m); b) Longitudinal**
 296 **profile along the channel centreline showing the original elevation derived from the Lidar DTM (black), and adjusted**
 297 **elevation (red). Comparison between observed (black) and simulated (red) time-series of water levels are shown at c)**
 298 **Pont Fawr, d) Trefriw, and e) Tal-y-Cafn.**

299 2.5 Idealised boundary conditions for model scenarios

300 The idealised model scenarios were used to add more detail to the historic records of flooding and instrumental data (Figures
301 2 and 3) to enable driver thresholds for flooding to be established. ~~Idealised scenarios are used to standardise the boundary~~
302 ~~conditions (Figure 5). Three scenarios, each consisting of 520 simulations, tested the influence of the relative drivers of estuary~~
303 ~~flooding (tidal water level, storm surge, river discharge, and time lag) – see Table 2 and Figure 5. The simulations consisted~~
304 ~~of 40 river discharge conditions with incrementally increasing Q_{max} , in combination with: (Scenario-1) 13 incrementally~~
305 ~~increasing tide levels combined with a maximum storm surge; (Scenario-2) 13 incrementally increasing tide levels combined~~
306 ~~with a mean storm surge; and (Scenario-3) 13 incrementally increasing tide levels combined with a maximum storm surge and~~
307 ~~a three-hour time lag. In total, $40 (Q_{max}) \times 13 (TWL_{max}) \times 3$ (scenarios) = 1,560 discrete simulations were performed. Each~~
308 ~~simulation was run for a period of 72 hours, allowing for model spin-up (thus allowing the assumed initial condition to become~~
309 ~~consistent with the hydrodynamic system) and with TWL_{max} and Q_{max} occurring after ~40 hours. These boundary conditions~~
310 ~~are described in more detail below.~~

311 2.5.1 River discharge

312 The following method was undertaken to generate 40 idealised discharge time series parameterised on the hydrology of the
313 Conwy. Firstly, a two-parameter gamma distribution was used to generate a synthetic series of normalised, idealised gamma
314 curves, that represent hydrograph shapes that cover the natural range of river flow behaviours experienced in the Conwy based
315 on 30 years of river discharge data from the Cwmlanerch river gauge (see Robins et al., 2018). The gamma curve with the
316 gradient of the rising hydrograph limb that most closely resembled the average gradient of the top 50 Q_{max} events analysed
317 in this study was selected. The selected idealised hydrograph had the largest gradient representing the flashiest flow behaviour.
318 The magnitude of the idealised hydrograph was then scaled to a peak discharge Q_{max} of 25 m/s (i.e., a relatively small river
319 flow event that will not likely cause flooding), with a base flow of 20 m/s which represents mean flow conditions. The scaling
320 of Q_{max} was successively increased from 25 m/s, in 25 m/s increments, up to a Q_{max} of 1000 m/s (i.e., slightly greater than
321 the maximum recorded event of 901 m/s), always keeping a base flow of 20 m/s). This created a realistic range of 40 river
322 discharge event time series that were applied to all three scenarios. For each simulation, Q_{max} occurred at 40 hours (Figure
323 5).

324 2.5.1-2 Total water level

325 The boundary conditions for total water level consisted of 13 time series for each of the three scenarios. These time series were
326 created using idealised ~~were created using predicted~~ tidal signals combined with residual surges. Firstly, a sinusoidal elevation
327 with a period of 12.42 hours (equivalent to the dominant M2 tidal constituent) was created. This was parameterised to represent
328 mean neap tides at Llandudno. Mean spring and neap tidal amplitudes and high tide levels were determined using a harmonic
329 analysis (T-Tide (Pawlowicz et al., 2002)), a package of routines that can be used to perform classical harmonic analysis, was

330 ~~used based~~ on 12 months of tide gauge data from Llandudno (2002-2003), ~~to calculate the amplitude of each tidal constituent.~~
331 A subsequent tidal prediction revealed that mean high water neap tides reach 1.82 m (OD) and mean high water spring tides
332 reach 3.6 m (OD) at ~~the Llandudno tide gauge for the 12-month period. The M2 tidal constituent has an amplitude of 2.71 m~~
333 ~~and was used to produce a constant sinusoidal curve for 72 hours. This was scaled initially to represent neap high tide levels~~
334 ~~at Llandudno. The elevation time series was then reproduced 13 times, each time. The procedure was then repeated by~~
335 successively increasing the ~~amplitude scale factor~~ so that high water was incrementally increased by 25 cm until equivalent
336 to spring high tides. ~~This experimental design purposely neglected the influence of other constituents so that the results were~~
337 ~~standardised. The model simulated the shallow water propagation of the tide advancing up the estuary, thus creating 13 water~~
338 ~~level time series.~~
339 ~~Secondly, for each of the three scenarios, a~~ residual surge was ~~then~~ added to the 13 ~~predicted tide~~ elevation time series to
340 represent the meteorological contribution to the total water level. ~~The shape of the surge was a~~ representative of typical storm
341 ~~conditions surge shape~~ for Llandudno (Environment Agency, 2016), ~~as shown in Figure 5. The surge~~ was shifted in time so
342 that the maximum surge height coincided with the fourth high tide (at around 40 hours). ~~For Scenario-1 and Scenario-3, the~~
343 ~~surge was and~~ scaled to the magnitude of the maximum observed skew surge (1.03 m). The resultant 72-hour time series
344 represented several tidal cycles where flooding was not expected (tide-only), followed by a tide + surge event at ~40 hours
345 (where the peak water level is denoted as *TWLmax*), before the regular tidal cycles resumed (Figure 5a and 5c). ~~For Scenario-~~
346 ~~2, (The procedure was then repeated, this time by applying a mean observed skew surge (0.13 m) to the predicted tide series~~
347 ~~(Figure 5b), thus creating an additional set of 13 tide + mean surge time series. The boundary conditions (from 20 to 60 hours)~~
348 ~~shown in Figure 5a illustrate the 13 tidal + maximum surge time series (collectively named Scenario-1), whereas those shown~~
349 ~~in Figure 5b illustrate the 13 tidal + mean surge time series (collectively named Scenario-2).~~

350 2.5.3 Time lag

351 The ~~relative~~ timing of *Qmax* relative to *TWLmax* is a key factor in determining compound flooding hazards. This time lag was
352 therefore considered in our sensitivity framework. From the 30-year Cwmlanerch discharge record, we calculated the
353 distribution of time lags (following the method of Lyddon et al., 2021), as shown in Figure 5d. Peaks in river discharge most
354 commonly occurred 0-4 hours before peaks in total water level, i.e., on the rising tide. Initially (~~described in Section~~
355 ~~2.5.2 Scenario-1 and Scenario-2~~), we implemented the most common time lag of 0 hours (i.e., both *Qmax* and *TWLmax* were
356 at 40 hours as shown in Figure 5a (Scenario-1) and Figure 5b (Scenario-2). Next, a -3 hour time lag was implemented as
357 shown in Figure 5c, since this was the next most common time lag (Figure 5d), and applied to the 13 tidal + maximum surge
358 time series and 40 discharge time series (collectively named Scenario-3). In total, $13 (TWLmax) \times 40 (Qmax) \times 3$ (scenarios)
359 = 1560 simulations of 72-hour duration were computed, as summarised in Table 2 and Figure 5.

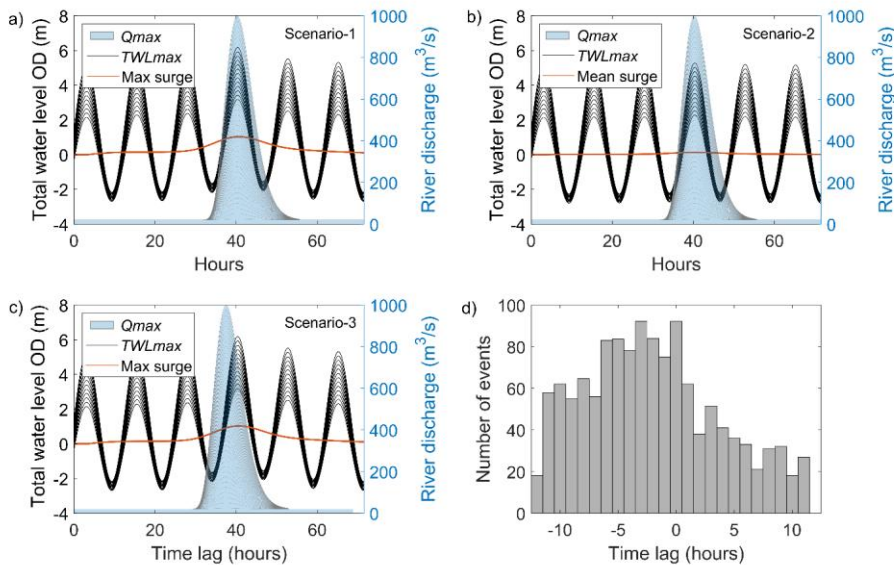
360
361 Table 2: Summary of model scenarios, each containing 520 combination simulations

Formatted: Font: Italic

Formatted: Font: Italic

Set of combination simulations	Peak total water level (TWL_{max})	River (Q_{max})	Time lag
Scenario-1	(Neap : 25cm : spring) + max surge = 1.03 m	25 : 25 : 1000 m ³ /s	0 hours
Scenario-2	(Neap : 25cm : spring) + mean surge = 0.13 m	25 : 25 : 1000 m ³ /s	0 hours
Scenario-3	(Neap : 25cm : spring) + max surge = 1.03 m	25 : 25 : 1000 m ³ /s	-3 hours

362
363



364

365 **Figure 5: Idealised model boundary conditions for a) Scenario-1, b) Scenario-2, and c) Scenario-3. Sea levels comprised**
366 **a) tidal + maximum surge with 0 hour time lag (at ~40 hours); b) tidal + mean surge with 0 hour time lag; c) tidal +**
367 **maximum surge with -3 hour time lag. Each scenario in (a-c) also shows 40 river discharge hydrographs with baseflow**
368 **of 20 m³/s and each with a successively increased river flow event with Q_{max} occurring at ~40 hours. d) Histogram of**

Formatted: Font: Italic

369 recorded time lag values between all Q_{max} at Cwmlanerch and TWL_{max} at Llandudno, spanning the period 1980-
370 2023.

Formatted: Font: Italic

Formatted: Font: Italic

371 2.6 Simulations of flooding

372 The following methodology was applied to identify the extent of flood extent under each scenario generated in section 2.5.

373 The flooding problem can be represented as a function:

$$374 \text{ FloodArea} = f(Q_{max}, TWL_{max}, SurgeHeight, Time Lag) \quad (1)$$

375 Where the *FloodArea* quantifies the inundation area (km²) of the Conwy estuary floodplains, as a function of Q_{max} (25 - 1000
376 m³/s), TWL_{max} (tidal + surge) (2.25 - 6 m), surge height (max = 1.03 m, mean = 0.13 m), and time lag (0, -3 hours), as
377 specified in Equation 1.

378

379 A high-performance computing system, Supercomputing Wales (<https://www.supercomputing.wales/>), was used to efficiently
380 run the Caesar-Lisflood solver. The system is capable of handling multiple concurrent computing tasks, to allow the parameter
381 space to be partitioned into 'job blocks'. Blocks were submitted to the system using the SLURM (<https://slurm.schedmd.com/>)
382 workload manager for batch processing. A typical 72-hour simulation took 1.2 – 2 hours of CPU runtime (on four Intel Xeon(R)
383 cores operating at 2.1 GHz). Overtopping of levees and shallow flows over floodplains can lengthen the computational time,
384 while dry parts of the catchment do not affect the computing time.

385

386 The output data comprises water depth grids in time layers with an interval of 15 minutes. Only data of time layers between
387 2300 and 3500 mins (~38–58 hours), corresponding to the period of widest flooding extents, were stored to reduce space.

388 Post-processing to summarise outputs and calculate *FloodArea* was completed remotely to reduce the transfer load from the
389 nodes to the local computer.

390 2.7 Scenario analysis

391 An initial baseline 'no flooding' simulation was performed, from which to calculate *FloodArea* in all subsequent simulations.
392 The baseline simulation represented moderate river flow and sea level conditions whereby water was contained within the
393 main channel, with dry floodplains, and high water levels submerged mid-channel shoals. The baseline was drawn from an
394 actual event in 27-Jan-2016, in which no inundation occurred. This case approximates the Scenario-1 simulation [Q_1TWL_3]
395 (i.e., $Q_{max} = 25$ m³/s, $TWL_{max} = 3.7$ m). A mask has been used to define the region of interest (ROI), see Figure 1a), an area
396 of 196×979 cells or ~7.7 km², which encompasses the estuary floodplains from the tidal limit at Cwmlanerch to the Conwy
397 Tunnel near the estuary mouth. Six mid-channel shoals were excluded with areas ranging from 0.003 km² to 0.17 km². The
398 baseline scenario comprises 13,982 wet cells in this ROI (~5.59 km²). For each simulation, the maximum total flooded area in
399 the ROI was recorded, from which the baseline 'no flood' wet area was subtracted to create the simulated *FloodArea*. A

400 floodplain model cell was considered to have flooded when the local water level exceeded a threshold of 2.5 cm. Wetted
401 surfaces need some time to drain, hence the variation in flooded areas lags behind the water level variations. Furthermore, the
402 minima of the flooded areas do not fully develop before the next flooding phase occurs. As experimented with a number of
403 scenarios accompanying the study, if the depth threshold was set as zero, any thin layer of water is considered inundation, and
404 then the flooded area is monotonically increasing (not shown here). Once the land is wet there is no way to change back into
405 dry. Only new events with higher water levels may expand the inundated area. This is a practical decision, but we also realise
406 that the flooding area is relatively insensitive when this depth threshold varies from 2.5 cm to 12.5 cm. The *FloodArea* for
407 each simulation was the inundated area exceeding this threshold. *FloodArea* and absolute difference in *FloodArea* (between
408 scenarios) are presented throughout the 520-simulation parameter space for [each of the Scenarios-1-3](#).

409
410 Spatial inundation maps were presented. Four cases were presented in this way, based on the Scenario-3 simulations: (i) TWL
411 dominated flooding; (ii) Q dominated flooding; (iii) moderate compound flooding, and (iv) extreme combined flooding. Spatial
412 variability in flooding was also presented as variations in lateral flood extent (in m) across east-west transects of the floodplains
413 at regular 20 m intervals, from the estuary mouth to the tidal limit —done this way since the Conwy is almost aligned in the
414 north-south direction (typical deviation in angle of $\pm 30^\circ$). Again, the four cases (i-iv) above were presented in this way for
415 lateral flood extent, based on the Scenario-3 simulations. For each case (i-iv), three simulations were presented with similar
416 *FloodArea*:- (i) TWL dominated, 3.1-6.5 km²; (ii) Q dominated, 11.13-11.8 km²; (iii) moderate compound, 5.4-8.3 km²; and
417 (iv) extreme compound, 8.8-9.1 km².

418 2.8 Estimating joint probabilities

419 [Joint probabilities are important in statistics, providing a way to model and analyse the simultaneous occurrence of events. In](#)
420 [the context of flood analysing, the joint probabilities identify the likelihood of combinations of coastal and river conditions](#)
421 [occurring, and capture relationships between variables \(Wu et al., 2021; Olbert et al., 2023; Moradian et al., 2023\). The joint](#)
422 [probability of river and sea level conditions can be interpreted in the context of i\) hydrodynamic model outputs to identify the](#)
423 [likelihood of combinations of conditions occurring to create a flood hazard, and ii\) recorded historic flood events to provide](#)
424 [context to the severity of flood events. Copulas are effective at modelling nonlinear dependence structures and joint distribution](#)
425 [between two variables. The copulas functions \(Sklar, 1959\) are used here to generate synthetic bivariate pairs of extreme sea](#)
426 [levels and river discharges, thus making their respective probability distribution more robust to apply joint probability methods.](#)
427 The Copula method was employed in this study to compute joint probabilities for extreme sea levels and river flows co-
428 occurring in the Conwy [for the first time](#). The joint probabilities were computed using the framework introduced by Sadegh et
429 al. (2017) and Moradian et al. (2023). The proposed framework uses three main components: (i) 16 statistical distributions
430 were employed to identify the best marginal distributions; (ii) 26 distinct Copula functions were applied to [sea level and river](#)
431 [flows](#)~~the data~~; and (iii) the Bayesian method was employed to compute the joint probabilities. The following sections provide

432 a concise overview of the steps involved in this framework, while more comprehensive details can be found in Sadegh et al.
433 (2017, 2018), Yazdandoost et al. (2020), and Moradian et al. (2023).

434 2.8.1 Statistical marginal distributions

435 To identify the most suitable marginal distributions for the data, researchers commonly employ parametric or nonparametric
436 distributions. It is important to note that each variable's marginal distribution is modelled using the best-fitted distribution, as
437 shown in Table 6 of Moradian et al. (2023). To assess the accuracy of the marginal distributions, their significance at a 5%
438 level is evaluated using the Chi-square goodness of fit test (Greenwood and Nikulin, 1996). Furthermore, various metrics are
439 used for statistical evaluations, as detailed in Table 5 of Moradian et al. (2023). These metrics include the Akaike information
440 criterion (AIC), Bayesian information criterion (BIC), Maximum likelihood estimation (MLE), Nash-Sutcliffe efficiency
441 (NSE), and Root mean square error (RMSE).

442 2.8.2 The Copula Method

443 Copula functions are mathematical functions that link or connect time-independent variables (Nelsen, 2007), irrespective of
444 their individual distribution characteristics (Genest and Favre, 2007). According to Sklar's theorem (Sklar, 1959), if we have
445 two continuous random variables X and Y with probability density functions of $f_x(x)$ and $f_y(y)$, and cumulative distribution
446 functions of $F_x(x)$ and $F(x)$, respectively, and if both have the same marginal distribution function F , then there exists a
447 unique Copula function: $C: [0,1]^2 \rightarrow [0,1]$ which serves as a bivariate cumulative distribution function and has uniform
448 margins:

$$449 F(x, y) = C(F_x(x), F_x(y)) \quad (2)$$

451 In an n -dimensional space, the cumulative distribution function F can be defined in terms of the Copula function C and the
452 marginal distribution functions as follows:

$$453 F(x_1, x_2, \dots, x_n) = C(F_1(x_1), F_2(x_2), \dots, F_n(x_n)) \quad (3)$$

454 where F_1, F_2, \dots, F_n are the marginal distribution functions (Nelsen, 2007).

455 A wide range of Copula functions are available, categorised into various families such as Gaussian, Plackett, Archimedean,
456 elliptical, and t families (Abbasian et al., 2015). Table 4 in Moradian et al. (2023) provides a compilation of the applied
457 Copula families and their corresponding mathematical descriptions. Here, to choose the best Copula family, different metrics
458 were used according to Table 5 in Moradian et al. (2023). In addition, the ~~dependence measures~~correlation coefficients for the

463 used flood pairs are Pearson's Linear Correlation Coefficient, Kendall's-Tau Correlation Coefficient and Spearman's Rho
464 Correlation Coefficient (Akoglu, 2018).

465 2.8.2 The Bayesian Method

466 The Bayesian-statistical method entails assessing the likelihood of an event, taking into account existing knowledge of
467 conditions that may be associated with the occurrence of the event. The concept has demonstrated remarkable success in
468 diverse fields, including hydrology (Sadegh et al., 2017) -and weather forecasting (Khajehi et al., 2017; Yazdandoost et al.,
469 2020).

470

471 ~~The joint probability distribution of A and B data in the Bayesian structure is written as follows:~~

472

$$473 \quad P(A|B) = \frac{P(A) \cdot P(B|A)}{P(B)} \quad (4)$$

474 where $P(A|B)$ is the probability of A being true, given B is true; $P(B|A)$ is the probability of B being true, given A is true; is
475 the probability of A being true and; $P(B)$ is the probability of B being true. Consequently, the utilisation of Copula functions
476 yields the joint probability distribution.

477 **3 Results**

478 Results are presented for simulated *FloodArea* for Scenarios-1-3 in the Conwy estuary (Sections 3.1 - 3.3), where a range of
479 1560 idealised simulations represent likely sea level and river flow 'compound storm events' that could lead to flooding. Next
480 (Section 3.4), for Scenario-3, a selection of simulated flooding maps and along-channel flooded width graphs are presented.
481 Finally (Section 3.5), joint probabilities are assigned to the compound flood drivers.

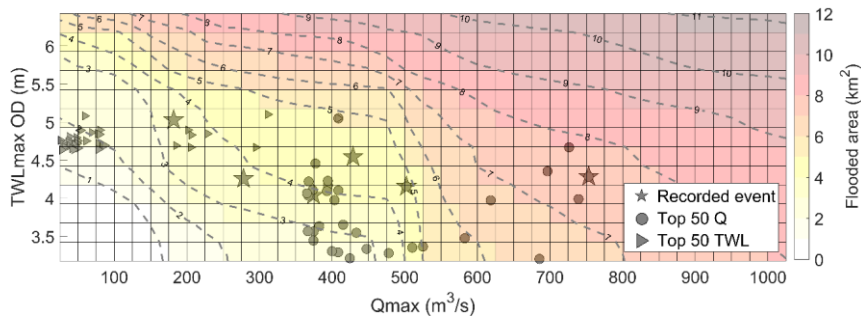
482 **3.1 Scenario-1 [tide series + max surge combined with river discharge series and 0 hour lag]:**

483 For Scenario-1, a surge tide event (skew surge = 1.03 m) was simulated, with a 0-hour time lag (i.e., Q_{max} and TWL_{max}
484 occurred simultaneously at 40 hours of the 72-hour simulations). The simulated *FloodArea* (km²) for all 520 simulations is
485 shown in Figure 6 where white represents little to no flooding, and red indicates maximum flood extent (> 10 km²). The top
486 50 Q_{max} and TWL_{max} events, and the recorded flooding events, are also shown. As expected, there was no or little (< 1 km²)
487 flooding simulated under the low-magnitude river flow and sea level events ($Q_{max} < 100$ m³/s and $TWL_{max} < 4$ m). Flooding
488 wasn't simulated with Q_{max} of 25 m³/s until TWL_{max} was 3.95 m, and then as Q_{max} was increased a reduced TWL_{max} was
489 needed to cause flooding. For example, flooding was simulated with $Q_{max} = 50$ m³/s and $TWL_{max} = 3.6$ m, as well as Q_{max}
490 = 100 m³/s and $TWL_{max} = 3.4$ m. *FloodArea* increased as Q_{max} and TWL_{max} increased. The simulated maximum *FloodArea*
491 was 11.2 km² under the $Q_{max} = 1000$ m³/s and $TWL_{max} = 10$ m combination.

492

Formatted: Normal

493 The contours shown in Figure 6 connect the model simulations with similar *FloodArea* (although not necessarily inundation
 494 of the same areas within the floodplains) and suggest a complex relationship between Q_{max} and TWL_{max} drivers in terms of
 495 simulated flooding. The contour gradients, shapes, and separation can therefore be interpreted to explain the dynamics of
 496 flooding. The contour gradients change across the range of simulations as *FloodArea* becomes more or less sensitive to one
 497 driver or the other. The 1 and 2 km² contours are broadly straight diagonals (bottom left part of Figure 6), as are the 9, 10 and
 498 11 km² contours (top right part of Figure 6). In these cases, *FloodArea* is broadly equally sensitive to both Q_{max} and TWL_{max}
 499 drivers. Convex contours (e.g. the middle sections of the 3 and 4 km² contours in Figure 6) indicate a compounding flood
 500 effect, as the addition of both drivers amplifies *FloodArea*. Conversely, concave contours (e.g. the middle sections of the 5-7
 501 km² contours in Figure 6) indicate a degressive flooding effect, where the combination of the drivers leads to relatively less
 502 *FloodArea*. There is a widening between the convex (4 km²) and concave (5 km²) contours in the centre of Figure 6, indicating
 503 that simulated flooding was relatively insensitive to changes in Q_{max} between 350 and 500 m³/s and TWL_{max} between 4 and
 504 5 m. Hence, several simulated compound event permutations within these driver ranges produced broadly similar *FloodArea*.
 505 Contours that are near horizontal (e.g. the 5 and 6 km² contours in the top left and middle parts of Figure 6) indicate that
 506 changes in flooding are predominantly driven by changes in TWL_{max} . Whereas contours that are near vertical (e.g. the 5 and
 507 6 km² contours in the bottom middle part of Figure 6) indicate that changes in flooding are predominantly driven by Q_{max} .
 508 Contours that are relatively close together (e.g. 5-7 km² contours where $TWL_{max} > 5.25$ m) potentially indicate key thresholds
 509 where small changes in one or both drivers lead to large changes in flooding.
 510



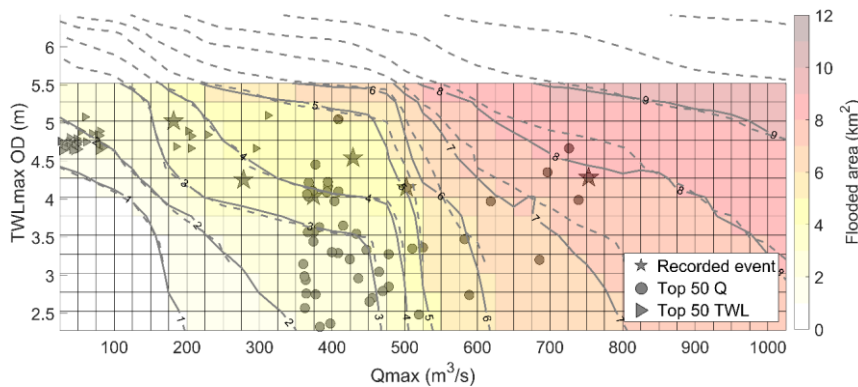
511
 512 **Figure 6: Scenario-1 (13 tide + max surge water levels combined with 40 river flow events, with 0 hr time lag): Coloured**
 513 **surfaces represent modelled *FloodArea* (km²) from combinations of 520 Q_{max} and TWL_{max} simulations. The contours**
 514 **link common *FloodArea* magnitude. Shapes correspond with Figure 2 and indicate extreme Q_{max} and TWL_{max} values**
 515 **within the historical record (NRW Recorded Flood Events (stars), top 50 TWL_{max} (triangles) and top 50 Q_{max}**
 516 **(circles)).**

- Formatted: Font: Italic
- Formatted: Font: Italic
- Formatted: Font: Italic
- Formatted: Font: Italic
- Formatted: Font: Italic
- Formatted: Font: Italic
- Formatted: Font: Italic
- Formatted: Font: Italic

517 **3.2 Scenario-2 [tide series + mean surge combined with river discharge series and 0 hour lag]:**

518 Scenario-2 simulated the effect on flooding of a mean surge magnitude, in difference to the maximum surge simulated in
519 Scenario-1. The difference from Scenario-1 in simulated *FloodArea* is shown in Figure 7, by subtracting *FloodArea* results of
520 Scenario-2 from Scenario-1. The *TWLmax* boundary conditions were lower for Scenario-2 (2.25-5.25 m) than for Scenario-1
521 (3.75-6.25 m), due to the smaller contribution of the surge, and gives insight into flooding dynamics under lower *TWLmax*
522 values. Both sets of scenarios have the same underlying M2 tidal signal, so the absolute difference in *FloodArea* is due to the
523 influence of the surge magnitude/shape for each scenario. All Scenario-1 simulations cause a larger *FloodArea* than Scenario-
524 2 simulations, for the same *Qmax* and *TWLmax* values. The influence of the different surge magnitudes/shapes on *FloodArea*
525 has the greatest impact under high *TWLmax* conditions (> 4.25 m), and with *Qmax* values below 500 m³/s, causing a variance
526 of up to 5 km² in *FloodArea*. Under low river and low sea level scenarios (bottom left of grid), or high river and sea level
527 scenarios (top right of grid), a larger surge consistently causes 2-3 km² more *FloodArea*.

528



529

530

531 **Figure 7: Scenario-2 (13 tide + mean surge water levels combined with 40 river flow events, with -0 hr time lag):**
532 **Coloured surfaces represent modelled *FloodArea* (km²) from combinations of 520 *Qmax* and *TWLmax* simulations. The**
533 **dashed contours link common *FloodArea* magnitude for scenario-2, whereas the solid contours refer to scenario-1 for**
534 **comparison. Shapes correspond with Figure 2 and indicate extreme *Qmax* and *TWLmax* values within the historical**
535 **record (NRW Recorded Flood Events (stars), top 50 *TWLmax* (triangles) and top 50 *Qmax* (circles)).**

536

Formatted: Font: Italic

Formatted: Font: Italic

Formatted: Font: Italic

Formatted: Font: Italic

Formatted: Font: Italic

Formatted: Font: Italic

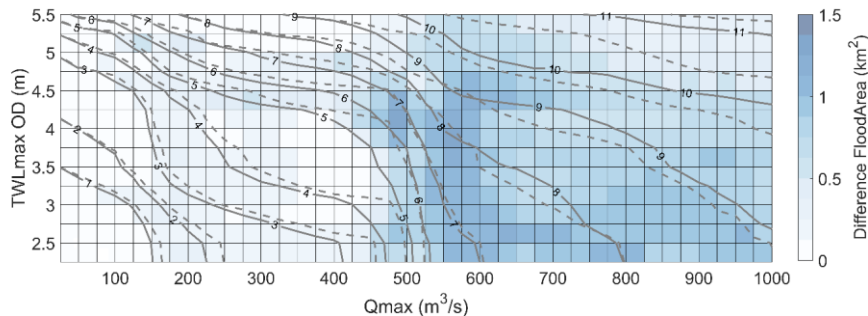
Formatted: Font: Italic

Formatted: Font: Italic

537 **3.3 Scenario-3 [tide series + max surge combined with river discharge series and -3 hour lag]:**

538 Scenario-3 simulated the effect on the flooding of a -3 hour time lag between Q_{max} and TWL_{max} , in difference to the 0 hour
 539 time lag simulated in Scenario-1 (both Scenarios simulated a maximum surge event). Differences in $FloodArea$ under an
 540 assigned -3 hours time lag (i.e. Q_{max} preceding TWL_{max} by 3 hours, hence occurring during flooding tide), compared with
 541 Scenario-1, are shown in Figure 8. Generally, a similar trend in flooding was simulated for both Scenarios and the gradients
 542 of the $FloodArea$ contours were similar (see also Figure S2 in the Supplementary Material). One interesting difference,
 543 however, was that lower magnitude drivers ($Q_{max} < 200 \text{ m}^3/\text{s}$, $TWL_{max} < 3 \text{ m}$) simulated a larger $FloodArea$ for Scenario-3
 544 than Scenario-1. The $FloodArea$ contours in Scenario-3 were smoother in shape than for Scenario-1, most notably on the 5
 545 and 6 km^2 contours. This could indicate a more compounding effect of the drivers with a -3 hour time lag, since the lag causes
 546 more of the river water on the rising limb of the hydrograph to be retained within the estuary by the flooding tide. The simulated
 547 $FloodArea$ was sensitive to the shift in time lag however with notable variation depending on simulations. The blue cells in
 548 Figure 8 indicate that the -3 hour time lag scenarios produced a greater $FloodArea$ than in Scenario-1. The -3 hour time lag
 549 had a small influence (generally $< 0.5 \text{ km}^2$) on $FloodArea$ for $Q_{max} < 425 \text{ m}^3/\text{s}$ across all TWL_{max} simulations. For $Q_{max} >$
 550 $425 \text{ m}^3/\text{s}$, the differences in $FloodArea$ were generally $> 0.5 \text{ km}^2$. The greatest difference in $FloodArea$ was 1.2 km^2 from the
 551 simulation with $Q_{max} = 475 \text{ m}^3/\text{s}$ and $TWL_{max} = 4.7 \text{ m}$. Differences in $FloodArea > 1 \text{ km}^2$ were also simulated for $Q_{max} =$
 552 $550\text{-}650 \text{ m}^3/\text{s}$ and $TWL_{max} < 5 \text{ m}$. For $TWL_{max} > 5 \text{ m}$ and $Q_{max} > 800 \text{ m}^3/\text{s}$, $FloodArea$ appeared less sensitive to the time
 553 lag (differences $< 0.5 \text{ km}^2$). However, for $TWL_{max} < 5 \text{ m}$ and $Q_{max} > 800 \text{ m}^3/\text{s}$, $FloodArea$ appeared more sensitive to the
 554 time lag (differences of $0.5\text{-}1 \text{ km}^2$), presumably because the stronger river discharges were able to counter the blocking effect
 555 of weaker tidal currents. Irrespective of the time lag, a Q_{max} of $475\text{-}600 \text{ m}^3/\text{s}$ was again shown as the river conditions where
 556 there is a marked change in $FloodArea$ and high sensitivity to Q_{max} . A -3 hour time lag produces a 7.7 % increase in flooding
 557 across the parameter space compared with Scenario-1; Scenario-1 produced a total of 3299 km^2 $FloodArea$, and Scenario-3
 558 produced 3553 km^2 $FloodArea$.

559



560

Formatted: Font: Italic

Formatted: Font: Italic

Formatted: Font: Italic

Formatted: Font: Italic

Formatted: Font: Italic

Formatted: Font: Italic

Formatted: Font: Italic

Formatted: Font: Italic

Formatted: Font: Italic

Formatted: Font: Italic

Formatted: Font: Italic

Formatted: Font: Italic

Formatted: Font: Italic

Formatted: Font: Italic

Formatted: Font: Italic

Formatted: Font: Italic

Formatted: Font: Italic

Formatted: Font: Italic

Formatted: Font: Italic

Formatted: Font: Italic

Formatted: Font: Italic

Formatted: Font: Italic

Formatted: Font: Italic

Formatted: Font: Italic

561 *Figure 8: Coloured surface represents the absolute difference in modelled FloodArea between Scenario-1 (maximum surge*
562 *with 0 hour lag) and Scenario-3 (maximum surge with -3 hour lag). The solid contours link common FloodArea magnitude*
563 *for scenario-3, whereas the dashed contours refer to scenario-1 for comparison.*

564 3.4 Spatial distribution of the flooded area

565 Aside from simulating the *FloodArea* considered in Sections 3.1–3.3, it is also important to specify where the simulated flood
566 water is distributed. To quantify the distribution of flooding in various parts of the estuary-catchment system, four cases were
567 considered:

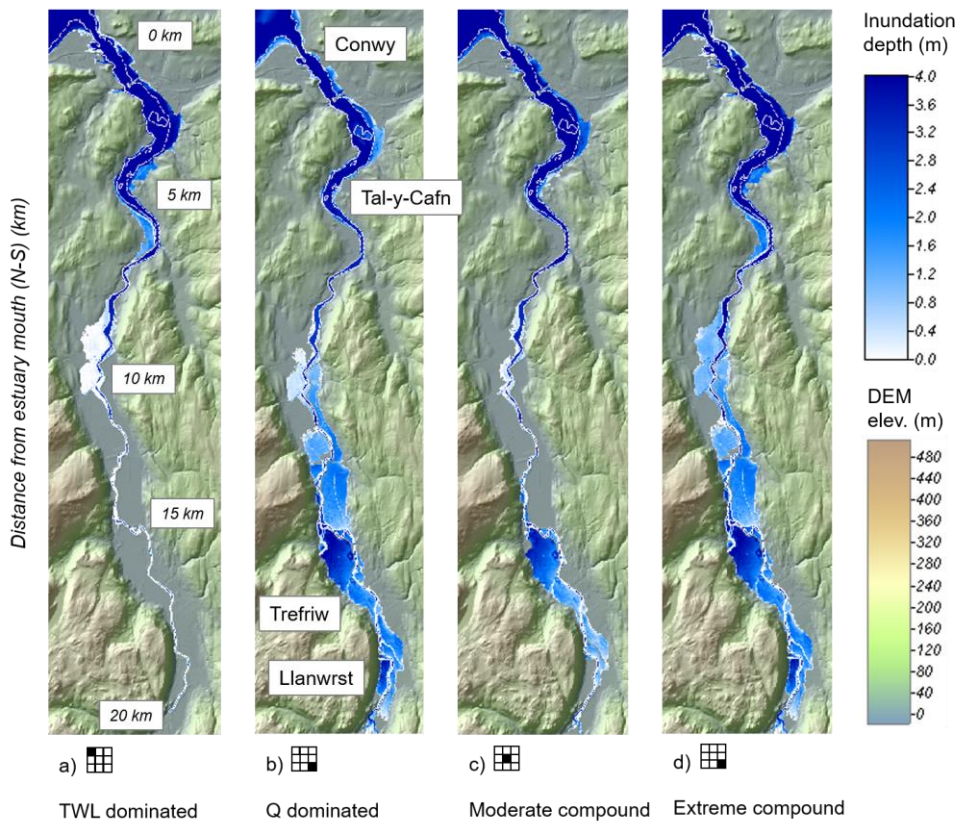
- 568 (a) TWL dominated: $TWL_{max} \geq 6.1$ m, $Q_{max} \leq 25$ m³/s.
- 569 (b) Q dominated: $TWL_{max} \leq 3.1$ m, $Q_{max} \geq 1000$ m³/s.
- 570 (c) Moderate compound: TWL_{max} 4.7–4.9 m, Q_{max} 475–500 m³/s.
- 571 (d) Extreme combined: $TWL_{max} \geq 6.1$ m, $Q_{max} \geq 1000$ m³/s.

572

573 Figure 9 shows the spatial distribution of flooding for the above four cases for Scenario-3 (tide + max surge combined with
574 river events and –3 hour time lag). The TWL-dominated event is shown in Figure 9a, where water inundated the lower and
575 middle estuary. The Q-dominated event simulated upstream flooding (Figure 9b). The moderate compound event is shown in
576 Figure 9c where the inundation pattern shows flooding mostly at the upstream region and part of the middle estuary. Finally,
577 the extreme combined event is shown in Figure 9d, where water inundated wide parts of the floodplains throughout the estuary.

578 It can be seen that the flooded region of [Figure 9d](#) is broadly the union of that in Figures 9a and 9b.

579



580

581

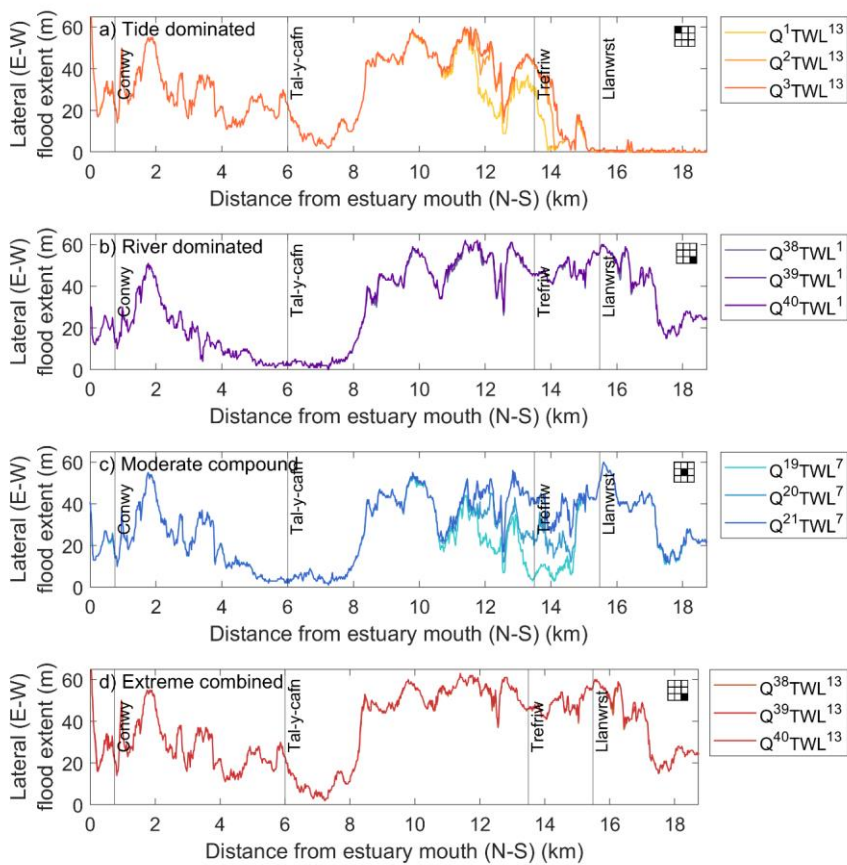
582 **Figure 9: Scenario-3 (tide + max surge with river events and -3 hour lag): Simulated maximum flooded extent (blue**
 583 **shades) of the region of interest for cases: (a) TWL-dominant (Q_1TWL_{13}), (b) Q-dominant ($Q_{40}TWL_1$), (c) Moderate**
 584 **compound ($Q_{20}TWL_7$), (d) Extreme combined ($Q_{40}TWL_{13}$). Corresponding *FloodAreas* are 5.6 km², 11.5 km², 8.9 km²,**
 585 **and 6.6 km², respectively. The icons show the relative position of each case (a-d) on the $TWLmax:Qmax$ parameter**
 586 **space (detailed in Supplementary Information). The white dashed lines delineate the shoreline in the ‘no flooding’**
 587 **basecase. The green-brown shading denotes dry land.**

588

Formatted: Font: Italic

Formatted: Font: Italic

589 The lateral extents of flooding, defined as the width of the inundated area in the direction perpendicular to the river channel,
590 for Scenario-3 for cases (a-d) are presented in Figure 10. In each case (a - d) three adjacent simulations are shown to depict
591 some driver sensitivity. For the TWL dominated case, the three simulations presented in Figure 10a show extensive lateral
592 inundation (15-60 m) simulated along the lower estuary floodplains (distance up to 6 km from the estuary mouth), with limited
593 inundation between 6-8 km, then extensive inundation further up-estuary (8-14 km) that was sensitive to Q_{max} (in the range
594 25-100 m³/s), and limited inundation beyond 14 km. For the three Q dominated cases (Figure 10b), extensive inundation (20-
595 60 m) was simulated in the upper estuary (8-19 km) with minimal sensitivity between the three simulations. For the moderate
596 compound event cases (Figure 10c), simulated lateral inundation showed large sensitivity to forcing conditions, with up to 40
597 m variability between the three simulations at 10-14 km. The capacity of the estuary for floodwater storage is clearly sensitive
598 in this region. Finally, for the extreme combined event cases (Figure 10d), extensive lateral flooding (15-60 m) was simulated
599 throughout the lower and upper estuary, except between 6-8 km where there was again limited flooding simulated. There was
600 little sensitivity (< 1 m) between the three simulations shown.
601



602
 603 **Figure 10: Scenario-3 (tide + max surge with river events and -3 hour lag): Distribution of lateral flooding along the**
 604 **Conwy estuary floodplain for four cases across the $TWL_{max}:Q_{max}$ parameter space: (a) TWL dominant ($Q_{1-3}TWL_{13}$);**
 605 **(b) Q dominant ($Q_{38-40}TWL_1$); (c) Moderate compound ($Q_{19-20}TWL_7$); and (d) Extreme combination ($Q_{38-40}TWL_{13}$).**
 606 **Lateral flooding is measured in the east-west direction. Along-estuary distance is measured in the north-south direction**

Formatted: Font: Italic

607 (from the estuary mouth to upstream). For each case (a-d), three simulations are presented (constant TWL_{max} and
608 varying Q_{max} - see also Figure S3). The icons show the relative position of each case (a-d) on the $TWL_{max}:Q_{max}$
609 parameter space (detailed in Supplementary Information).

Formatted: Font: Italic

Formatted: Font: Italic

Formatted: Font: Italic

610 3.5 Assigning probability to flood drivers

611 Figure 11 shows joint probabilities calculated from observed total water level at Llandudno and river discharge at Cwmlanerch,
612 presented on the $TWL_{max}:Q_{max}$ parameter space and overlaying the distribution of extreme events in the historic record.

Formatted: Font: Italic

613 Figure 11 represents a novel approach to interpreting joint probabilities in the context of historic storm events, to better
614 understand the relationship between drivers and impacts of flooding. The joint probabilities highlight the likelihoods and

615 severities of the historic extreme compound events. There were seven historic events which have a probability of <0.01 ,
616 indicating less than 1 event in 100 years of this magnitude, six of which are recorded as causing flooding (yellow circles),

617 whereas for one of these events no flooding was recorded (blue triangle). The no flooding event was 10 February 1997; Q_{max}
618 was $311 \text{ m}^3/\text{s}$ which peaked 1 hour 30 minutes before TWL_{max} , recorded as 5.1 m, including a 0.48 m skew surge. Reports

Formatted: Font: Italic

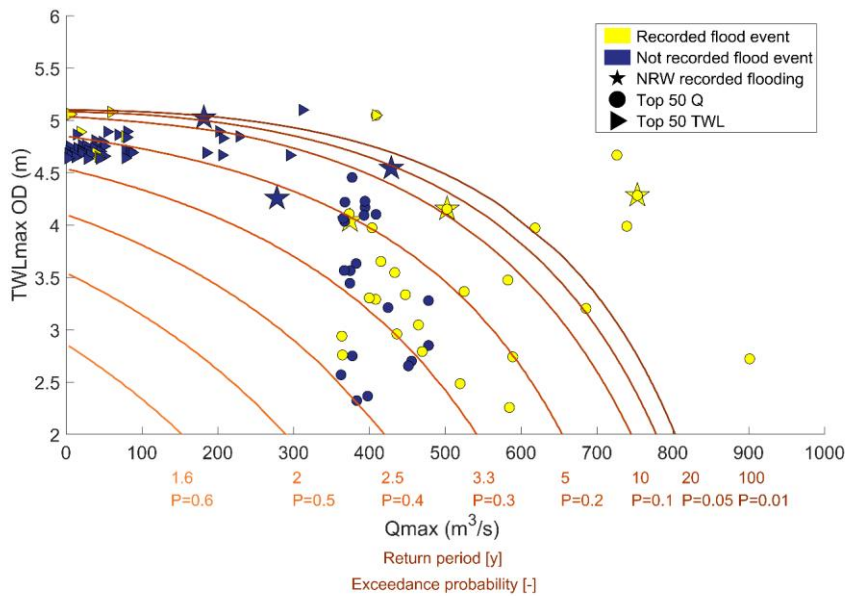
Formatted: Font: Italic

619 indicate this was a high water level event, associated with a 5 year sea-level return period, but these conditions did not cause
620 flooding or no flooding was recorded (HR Wallingford, 2008). This method allows return periods to be assigned to historic

621 extreme events and recorded flood events, and to estimate the likelihood and severity of potential future events. Figure 11
622 shows that the same joint probability can occur from a range of combinations of Q_{max} and TWL_{max} conditions. For instance,

623 an event with a 0.2 exceedance probability (1 event in 5 years) can occur on a TWL dominated, Q dominated, or moderate
624 compound event.

625



626
 627 **Figure 11: Joint probabilities for TWL_{max} and Q_{max} in the Conwy Estuary, where P = exceedance probability, ranging**
 628 **from high likelihood of co-occurrence ($P=0.6$) to low likelihood of co-occurrence ($P=0.01$) overlaid the distribution of**
 629 **extreme events (recorded and not recorded flooding) in the historic record.**

Formatted: Font: Italic

Formatted: Font: Italic

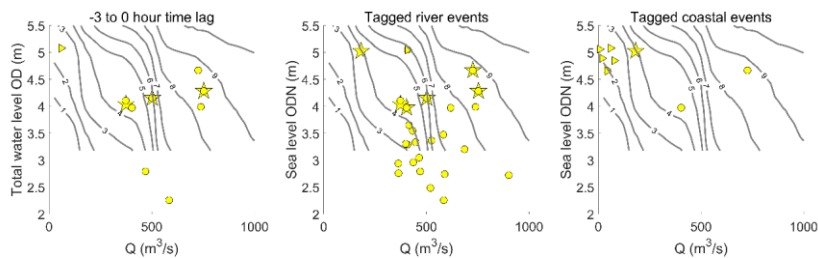
630 **4 Discussion**

631 This research ~~aims to has~~ established site-specific driver-thresholds for flooding in an estuary environment, using
 632 ~~hydrodynamic modelling. The simulations have been verified and contextualised using~~ documented records of flooding,
 633 ~~together with instrumental data analysis, hydrodynamic modelling, and statistical analysis of instrumental gauge time series,~~
 634 ~~approaches.~~ With application to the Conwy estuary, N-Wales, ~~the instrumental data and documented records of flooding have~~
 635 ~~been supplemented with simulated flooding using a validated~~ hydrodynamic inundation model ~~and was~~ applied to a series of
 636 idealised combined river and sea level compound events. ~~We show that flooding is co-dependent on TWL_{max} , Q_{max} , and their~~
 637 ~~relative time lag, and that historic records of flooding can be used to set driver and flood extent thresholds that isolate minor~~
 638 ~~and severe flooding. Below, Here~~ we discuss the ~~thresholds of flooding and the~~ importance of accurate records of historic

639 flooding events. We consider ~~which can be used in combination with modelling to identify thresholds for flooding, and~~
640 ~~consider how~~ these thresholds may change under different driver behaviours and combinations, and future climate conditions.

641 4.2.1 Thresholds for flooding

642 Since there are multiple drivers of flooding in estuaries, single-value driver-thresholds cannot be used, e.g., for the Conwy
643 estuary we show for the first time that flooding is co-dependent on TWL_{max} , Q_{max} , and their relative time lag. The simulated
644 flooding presented in Section 3 shows the total inundation ($FloodArea$) across the estuary system and includes both minor or
645 nuisance flooding up to severe flooding. Recorded ~~flood~~-events of flooding are isolated based on time lag and associated web
646 scraped tag(s) (cf. Section 2.3), and presented with $FloodArea$ contours from Scenario-3 to identify if there is a simulated
647 $FloodArea$ threshold that matches the recorded flooding events (Figure 12). The 2 or 3 km^2 contour lines can be interpreted as
648 a minimum $FloodArea$ contour for recorded flooding in the Conwy. The coastal events (Figure 12c) occur under high sea level
649 and across a range of river discharge combinations, indicating thresholds for flooding in the coastal zone should consider sea
650 level as the dominant driver. and thresholds may not need to consider this driver.

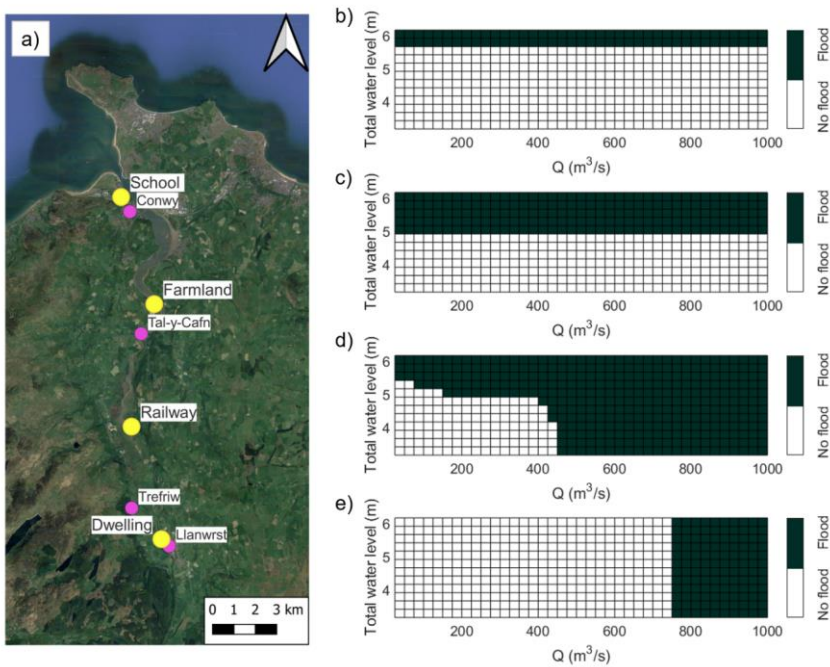


652 **Figure 12: Recorded flood events with a) a time lag between 0 to -3 hours; b) with tag [1] for river event; c) with web-**
653 **scraped keywords (tags) [3 4] for coastal event, all presented with $FloodArea$ contours from scenario-3.**

Formatted: Font: Italic

654
655
656 Whilst the $FloodArea$ representation gives a good overall perspective of flooding dynamics, a different approach is needed to
657 establish co-dependent driver-thresholds for flooding at different locations within the estuary. For a chosen location, as a first
658 step, a flood-threshold (i.e., depth of inundation) has to be established. For instance, one might expect to assign a different
659 flood-threshold for an area of unused woodland than an agricultural field or a dwelling or road, based on socio-economic
660 impact metrics (Cutter et al., 2013; Alfieri et al., 2016). Next, the inundation modelling shown in Section 3 can be used to
661 predict whether flooding is likely to have occurred or not for the range of compound events within the parameter space, and
662 hence define the site-specific co-dependent driver-thresholds. This is an approach often used for coastal infrastructure,
663 including nuclear sites (e.g. ONR, 2021) but rarely extended to individual properties or land users. We have demonstrated this
664 procedure below for four discrete locations within the Conwy estuary floodplains: (i) primary school, Conwy, (ii) farmland,

665 mid-estuary; (iii) section of railway, mid-estuary; and (iv) dwelling, Llanwrst. We used Scenario-3 (tide + max surge combined
 666 with river events with a -3 hour time lag) for this demonstration since this scenario predicted the most flooding. Figure 13
 667 shows the co-dependent driver-thresholds for each location (i-iv). Figure 13 shows TWL dominated flooding in the lower
 668 estuary when sea level > 5.7 m at the school and > 4.9 m at farmland, and river dominated flooding in the upper estuary at
 669 dwellings when river discharge > 750 m³/s. This also aligns with what is shown in Figure 10, and single variable (Q or TWL,
 670 respectively) flood probability analysis may be appropriate in these locations. Moderate compound flooding in the mid-estuary
 671 shows flooding under a wider range of TWL and Q combinations, and shows that joint probability analysis is necessary when
 672 both drivers influence flood magnitude.
 673



674
 675 **Figure 13: Site-specific flood thresholds to show the conditions that cause flooding to occur or not within the Conwy**
 676 **Estuary (a) using model outputs from Scenario-3 at: (b) primary school in lower estuary; (c) farmland in lower estuary;**
 677 **(d) railway in mid estuary; and (e) dwelling in upper estuary. [Figure 13a Basemap © OpenStreetMap 2023](#)**

678 **4.2.1.1 Flood dynamics related to driver magnitude & timing**

679 We show that flood forecasts need to be sensitive to both fluvial and sea level drivers of flooding in the Conwy Estuary, N-
680 Wales, particularly under medium levels (45-60th percentiles) of river discharge and total water level. Flood hazard assessments
681 must consider a bivariate approach to both river discharge and sea levels across an estuary, otherwise univariate approaches
682 will not appropriately characterise the hazard and will underestimate compounding effects (Moftakhari et al., 2017). Combined
683 river and sea level simulations show that when the drivers are extreme (e.g. > 85th percentile), they act equally and consistently
684 produce the highest magnitudes of flood inundation irrespective of their relative timing. The volume of riverine freshwater is
685 the dominant driver contributing to high water levels in the estuary. This could be evidence of the backwater effect, where
686 high river discharge can push back low levels of tidal water, resulting in a temporary increase in water levels within the estuary
687 (Ikeuchi et al., 2015; Feng et al. 2022).

Formatted: Superscript

688
689 ~~Results show that It is when the river discharge is between 450-550 m³/s in the Conwy Estuary that~~ flood forecasts need to be
690 particularly accurate for Conwy Estuary when the river discharge is between 450-550 m³/s, which represents moderate
691 conditions. We show that within this range of discharge there is considerable variability in flood inundation across a range of
692 sea-level magnitudes, and also sensitive to the timing of Q_{max} relative to TWL_{max} . This critical range of discharge values,
693 between 450 - 550 m³/s, could be related to the holding capacity of the estuary as there may be storage volume for flood water
694 below these magnitudes of discharge. This critical range of discharge values also represents a threshold for a change in the
695 behaviour of the drivers. Analysis of *FloodArea* contour shapes/gradients superimposed on historic flood inundation records
696 shows that compound effects are most significant under medium levels of river discharge and sea level. Below these medium
697 levels, then one or the other driver is more dominant. Above this level, then both drivers are equally dominant in their
698 contribution to flooding. These insights show that both drivers must be considered as dependent and interacting in flood
699 forecasts, to ensure that compound flood effects are captured and planned for.

Formatted: Font: Italic

Formatted: Font: Italic

700
701 An analytical model has been used in an idealised, meso-tidal estuary to show that there is always a point where river discharge
702 effects on water level outweigh tide-surge effects (Familkhalli et al., 2022). Non-linear effects and interactions between sea
703 level and river discharge can influence compound effects, including tidal damping, and tidal blocking, influence the location
704 at which river flow effects are larger than marine effects, or vice versa (Cai, 2014; Hoitnik and Jay, 2016; Xiao, 2021). The
705 magnitudes at which river discharge and sea level will cause compound effects to amplify flood inundation will vary between
706 estuaries. These effects may not occur in some estuaries, and be more extreme in others (Harrison et al., 2022). It is likely that
707 a range of factors will control this including tidal range, substrate type and bed friction, coastline aspect, estuary geometry and
708 size, catchment size, type and geology, river network, river transmission times, prevailing weather conditions, antecedent
709 weather, and local climate (Familkhalli et al., 2022). The parameter space could be developed by considering additional
710 hydrograph time lags, and exploring the timing of the surge relative to tidal high water which could influence the magnitude

711 and volume of the total water level (Lyddon et al., 2018; Khanam et al., 2021). The lag time is currently presented as between
712 *Q_{max}* and *TWL_{max}*, however there could be asymmetries within the estuary that prevent tidal slack water occurring at
713 *TWL_{max}*. The *Q_{max}* lag relative to slack tide (e.g. turning from flood to ebb) could be explored, however significant 3D lateral
714 flows in the Conwy Estuary (e.g. Robins et al., 2012; Howlett et al., 2015) would mean that identifying location and timing of
715 slack water would require a 3D baroclinic model. These additional parameters could alter the position, shape, or angle of
716 threshold contours, or understanding of flood dynamics. A better understanding of estuarine thresholds can enhance how
717 managers and engineers plan coastal protection strategies, including where to place defences, infrastructure, and buildings.

718

719 4.1 Documented records of flooding

720 Historical records of flooding in the Conwy estuary are incomplete, with few flooding events pre-2004 documented and
721 available online. More recent flooding events have only been recorded online unsystematically in a piecemeal fashion and are
722 contingent on the severity of the impact, suggesting that smaller flooding events or flooding away from people and
723 infrastructure have potentially been undocumented. Additionally, documented flooding events tend to focus on the impacts
724 rather than the drivers that caused the hazard. This study adds to the historical catalogue of flooding in the Conwy eEstuary by
725 collating all available documented events into one space together with the driving river flow and sea level conditions and their
726 relative timings. We believe that similar circumstances of incomplete historical records of estuary flooding are widespread
727 nationally and indeed there is limited knowledge of how estuary flooding has varied geographically. National UK chronologies
728 of flash flooding (Archer et al., 2021) and coastal flooding (Haigh et al., 2015) have been compiled, but such records do not
729 exist for estuaries.

730

731 Documenting compound flood events aids in understanding and analysing the drivers, interactions, and impacts of the hazards
732 (Haigh et al., 2015; Haigh et al., 2017), validating numerical and statistical techniques, and calculating optimal thresholds.
733 Recording historic information on river flows/levels, sea levels, other sources such as pluvial and groundwater flows, and
734 subsequent flooded areas helps to identify high-risk areas and areas where appropriate measures to reduce future flood risk
735 may be required. This prior knowledge combined with current information on where and when certain combinations of extreme
736 conditions are forecast can aid in incident response for flood agencies and emergency services, and help local authorities
737 identify what resources are needed in the short and longer term following flooding. Comprehensive historic flooding records
738 can provide an opportunity to assess the effectiveness of existing flood management policies and flood control measures, such
739 as floodwalls or drainage systems, that need improvement. This knowledge can guide future engineering designs for a range
740 of coastal development, ensuring the construction of more resilient and adaptive infrastructure that can better withstand flood
741 events. Documenting flood events can also build a database of information to help to raise public awareness of and resilience
742 to flood hazards. Photographs, videos, and written accounts of past events can evoke an emotional response to prompt
743 individuals and communities to engage with future flood preparedness and evacuation plans (Fekete et al., 2021; Wolff, 2021).

Formatted: Space After: 12 pt

744 This data could also be extended to include storm tracks, storm footprints, rainfall intensity, groundwater levels, and catchment
745 saturation to build a greater understanding of the meteorological conditions that can contribute to compound flooding events
746 (Zong et al., 2003). Social media data, including geolocated tweets, have been used to identify the remarkability of events and
747 highlight major cities, including Miami, New York, and Boston, that are vulnerable to flooding (Moore and Obradovich, 2020).
748 Qualitative hazard data from archived and digitised newspaper articles has been extracted to identify geographic location, date,
749 triggers and damages of estuarine floods (Rilo et al., 2022) and validate flood models (Yagoub et al., 2020).

750 The combined approach to identify driver-thresholds for compound flooding presented here, and additional parameters
751 suggested to develop the approach, relies on availability and access to sufficient instrumental data at the appropriate temporal
752 resolution, and topographical and bathymetric data at appropriate spatial resolution. The UK sea levels, river discharges, and
753 topography are recorded, archived, and accessed via national government and research agencies (e.g. British Oceanographic
754 Data Centre, National River Flow Archive, Centre for Environment, Fisheries and Aquaculture Science, and Channel Coastal
755 Observatory). However, nearly 50% of the world's coastal waters remain unsurveyed (IHO C-55, 2021), and 290 tide gauges
756 that form the Global Sea Level Observing System (GLOSS, Merrifield et al., 2009) are unevenly distributed across the globe
757 and do not account for local, vertical land movements. The approach described here could supplement existing observation
758 systems with new technologies to improve records of coastal processes (Marcos et al., 2019), at local scales including X-band
759 radar derived intertidal bathymetries (Bell et al., 2015; Bird et al., 2020), X-band radar derived tide and surge (Costa et al.,
760 2022), and regional scales including Satellite-Derived Bathymetry (Cesbron et al., 2021 and Hasan and Matin, 2022), and
761 satellite altimetry (Cipollini et al., 2019), which measures the sea level from space with sufficiently dense global coverage.
762 Global model projections of storm surge and tide can be downscaled and applied to inform assessment of coastal flood impacts
763 (Muis et al., 2023). Temporal and spatial gaps also occur in the global river discharge observing network, and hydrometric
764 data are not available in real time (Lavers et al., 2019; Harrigan et al., 2020). Research has focused on coupling surface and
765 sub-surface runoff models, hydrologic models, and land surface models, forced with global atmospheric reanalysis (e.g.
766 ECMWF's ERA5) to produce river discharge reanalysis (Harrigan et al., 2020). Combining observation and downscaled
767 modelled data to explore thresholds for estuarine flooding is one approach to apply this methodology worldwide.

768 Improving the resilience and preparedness of communities to flood hazard is a UK priority policy, as outlined in the Defra
769 Policy Statement on Flooding (2020), and highlights the need for integrated approaches to flood hazard management.
770 Instrumental data can be used in conjunction with earth observation records, including remote sensing and satellite imagery,
771 of flooding to build more comprehensive databases of past records of estuarine flooding and be supported with numerical
772 modelling studies to help identify thresholds for flooding (Heimhuber et al. 2021; Costa et al. 2023).-

773

774 4.3 Future changes in flooding

775 Extreme sea levels for the Conwy, comprising large spring tides and large skew surges, could reach ~6 m (OD) and were
776 simulated here in the upper rows of the scenario parameter space. These levels have not yet been seen in the Conwy but could
777 happen presently. The *FloodArea* contours are close together in this section of the parameter space and show that relatively
778 small increases in sea level and/or river flows lead to large increases in flood extent . This section of the parameter space is
779 likely to become more relevant in the coming decades, as a result of sea-level rise and projected increases in the magnitudes
780 of peak river flow events under future climate conditions. Sea-level rise and geomorphic changes will lead to a new baseline
781 for flooding and new driver-thresholds and interactions. Many studies have started to consider the impact of climate change
782 on compound estuary flooding (Robins et al., 2016; Ghanbari et al. 2021). Outputs of climate models were analysed to show
783 that changes in sea level and precipitation can substantially increase the likelihood of a compound event, where a 100-year
784 event could become a 3-year event by 2100 (Sheng et al., 2022). Model simulations of synthetic storms of combined tropical
785 cyclones and sea-level rise in Cape Fear Estuary, North Carolina, have shown that future climatology will increase a 100-year
786 flood extent by 27 % (Gori and Lin, 2022). In addition to future changes in drivers of compound events, it is possible that
787 changes in storm tracks will influence the clustering and timing of events (Haigh et al. 2016; Eichentopf et al. 2019), and
788 changes in land use could influence groundwater saturation, baseflow, and overall floodwater storage and drainage capacity
789 of the system (Rahimi et al., 2020). However uncertainties in future UK projections of river discharge and sea-level must be
790 accounted for when considering compound flood effects (Lane et al., 2022). It is beyond the scope of this research to explore
791 the influence of future climate changes on thresholds but could be explored by running simulations with different groundwater
792 saturation, clustered events, and higher sea level or river discharge behaviours. A better understanding of how compound
793 events and thresholds will change in the future is also crucial for developing adaptive strategies for high-impact events
794 (Zscheischler et al., 2018), and climate projections of changing sea level, storm surge, river discharge, and storm tracks should
795 be considered in model scenarios.

796 5 Conclusion

797 The urbanisation and industrialisation of estuaries have increased the vulnerability of communities to extreme events, such as
798 flooding from high sea levels and river discharge. The impacts of these events are further amplified when extreme sea/river
799 events occur simultaneously. Flooding occurs when coastal or fluvial conditions exceed critical thresholds such as flood
800 defence heights, so there is a need to identify the driving land and sea conditions under which these thresholds are exceeded
801 and the type of flooding that ensues. This research developed a novel framework that utilised a combination of historic estuary
802 flooding records, instrumental monitoring data, numerical modelling, and probabilistic analyses to identify driver-thresholds
803 for compound flooding, for an estuary that is especially vulnerable to compound flooding events (Conwy, N-Wales, UK).

804

805 ~~The research highlighted the incomplete nature of recorded flooding extents held by national agencies, which are important to~~
806 ~~build a database of past episodes of flooding (e.g., when and where has flooded, and under what conditions) and undertake~~
807 ~~further analyses such as temporal trends in flooding. Such a database is crucial for developing accurate and timely flood~~
808 ~~warnings. The historic flooding record for the Conwy was supplemented with information obtained from online sources~~
809 ~~available 2004-2022, and set within the context of the most extreme 100 compound events during the period 1980-2022. An~~
810 ~~estuary inundation model was then used to 'fill' the parameter space of possible compound events (1560 separate simulations).~~
811 ~~This combined approach of modelling referenced to historic flooding events allowed us to identify a range of thresholds for~~
812 ~~flooding.~~

813
814 The simulations predict how the total estuary flooding extent responds to the magnitude of river discharge, tide, and surge
815 magnitude, and the timing of peak river discharge relative to tidal high water. Most flooding occurs when one or both sea level
816 and river discharge drivers are extreme (e.g., >85th percentiles), but with amplified (compounding) flooding under relatively
817 moderate circumstances (e.g. 60-70th and 30-50th percentiles) and in specific regions of the estuary (mid-estuary). Flooding is
818 sensitive to a change in the timing of peak river discharge relative to tidal high water, with a -3 hour time lag (peak river
819 discharge three hours before high water and coinciding with a rising tide that 'traps in' the freshwater) causing 7.7 % more
820 flooding across the parameter space than with a 0 hour lag. There is spatial variability in flooding that is dependent on the
821 combination and magnitude of the drivers. We show in detail the simulated extent of flooding in the lower estuary under
822 extreme sea level conditions, and in the upper-estuary from extreme river flow conditions – and the spatially intricate nature
823 of flooding throughout the estuary under combined moderate and extreme ('worst-case') sea level and river flows.

824
825 The research highlights that the recorded flooding extents held by national agencies are incomplete. This database is important
826 to build knowledge on past flooding episodes (e.g., when and where has flooded, and under what conditions), undertake further
827 analyses such as temporal trends in flooding, and develop accurate and timely flood warnings. The historic flooding record for
828 the Conwy was supplemented with information obtained from online sources available 2004-2022, and set within the context
829 of the most extreme 100 compound events during the period 1980-2022. An estuary inundation model was then used to 'fill'
830 the parameter space of possible compound events (1560 separate simulations). This combined approach of modelling
831 referenced to historic flooding events allowed us to identify a range of thresholds for flooding.

832
833 The results highlight under which conditions flooding is predicted to occur, or not, throughout the estuary, and identify driver-
834 thresholds for flooding that are relevant to historic recorded flooding, steep increases in flooding (sensitive tipping-points),
835 and location-specific/impact-specific flooding. The method can be used to enhance our understanding of estuarine flooding
836 dynamics and improve flood risk assessments – it can be applied to other estuaries worldwide where there are paired coastal
837 and fluvial monitoring/model data, and the methodology can be developed to include additional drivers and changes in the
838 timing of behaviour of the drivers surges under different climate/management conditions.

839

840 **Code availability**

841 All code can be provided by the corresponding authors upon request.

842

843 **Data availability**

844 All raw data can be provided by the corresponding authors upon request.

845

846 **Author contribution**

847 CL, ~~CNNC~~, GV, PR, AB, and TC formulated the research and developed the methodology; GV and TC developed, calibrated,
848 and validated the model setup; ~~CN-NC~~ ran the model and managed model outputs; AO, SM, MR contributed to data analysis;
849 CL, ~~CNNC~~, and PR analysed and visualised results; CL wrote the manuscript draft; PR, ~~CNNC~~, GV, AB, TC, ~~IO-AO~~
850 contributed to, reviewed, and edited the manuscript.

851

852 **Competing Interests**

853 The authors declare that they have no conflict of interest.

854

855 **Acknowledgements**

856 The authors wish to acknowledge the NERC-UK Climate Resilience Programme project ‘SEARCH (NE/V004239/1)’, in
857 partnership with Jason Lowe, Rachel Perks, Jonathan Tinker, and Jennifer Pirret at the Met Office; Mark Pugh at Natural
858 Resources Wales; Sue Manson and Harriet Orr at the Environment Agency; and Fiona McLay at the Scottish Environment
859 Protection Agency. The authors also acknowledge Cllr Aaron Wynne at Conwy County Borough Council and John Owen and
860 Robert Meyer who are residents and landowners in the Conwy floodplains, for their knowledge on flooding in the region.

861

862 **References**

- 863 Abbasian, M.S.; Jalali, S.; Mousavi Nadoushani, S.S.: Multivariate Flood Frequency Analysis Using Copula with Parametric
864 and Nonparametric Marginal Distribution Function. MCEJ., 14 (4), 81-92, <http://mcej.modares.ac.ir/article-16-10840-en.html>,
865 2015.
- 866 Alfieri, L., Feyen, L., Salamon, P., Thielen, J., Bianchi, A., Dottori, F., and Burek, P.: Modelling the socio-economic impact
867 of river floods in Europe. Nat. Hazards Earth Syst. Sci., 16, 1401–1411, <https://doi.org/10.5194/nhess-16-1401-2016>, 2016.
- 868 Alfieri, L., Salamon, P., Pappenberger, F., Wetterhall, F., and Thielen, J.: Operational early warning systems for water-related
869 hazards in Europe, Environmental Science & Policy, 21, 35–49, <https://doi.org/10.1016/j.envsci.2012.01.008>, 2012.

870 Akoglu, H.: User's guide to correlation coefficients, Turkish Journal of Emergency Medicine, 18, 91–93,
871 <https://doi.org/10.1016/j.tjem.2018.08.001>, 2018.

872 Archer, D., O'Donnell, G., Lamb, R., Warren, S., and Fowler, H. J.: Historical flash floods in England: New regional
873 chronologies and database, J Flood Risk Management, 12, <https://doi.org/10.1111/jfr3.12526>, 2019.

874 [Arns, A., Wahl, T., Wolff, C., Vafeidis, A. T., Haigh, I. D., Woodworth, P., Niehüser, S., & Jensen, J.: Non-linear interaction
875 modulates global extreme sea levels, coastal flood exposure, and impacts. Nature Communications, 11\(1\),
876 <https://doi.org/10.1038/s41467-020-15752-5>, 2020.](https://doi.org/10.1038/s41467-020-15752-5)

877 Bates, P. D., Horritt, M. S., & Fewtrell, T. J.: A simple inertial formulation of the shallow water equations for efficient two-
878 dimensional flood inundation modelling. Journal of Hydrology, 387(1-2), 33-45.
879 <https://doi.org/10.1016/j.jhydrol.2010.03.027>, 2010.

880 BBC: National Eisteddfod: Flooding worries over Llanrwst site: <https://www.bbc.co.uk/news/uk-wales-47666319>, last access:
881 April 2023, 2019.

882 BBC: Storm Ciara: Dramatic scenes across Wales: <https://www.bbc.co.uk/news/uk-wales-51434782>, last access: April 2023,
883 2020.

884 Bilskie, M. V. and Hagen, S. C.: Defining Flood Zone Transitions in Low-Gradient Coastal Regions, Geophysical Research
885 Letters, 45, 2761–2770, <https://doi.org/10.1002/2018gl077524>, 2018.

886 [Bird, C.O., Bell, P.S., Plater, A.J.: Application of marine radar to monitoring seasonal and event-based changes in intertidal
887 morphology. Geomorphology, 285, 1–15, <https://doi.org/10.1016/j.geomorph.2017.02.002>, 2017.](https://doi.org/10.1016/j.geomorph.2017.02.002)

888 Camus, P., Haigh, I. D., Nasr, A. A., Wahl, T., Darby, S. E., and Nicholls, R. J.: Regional analysis of multivariate compound
889 coastal flooding potential around Europe and environs: sensitivity analysis and spatial patterns, Nat. Hazards Earth Syst. Sci.,
890 21, 2021–2040, <https://doi.org/10.5194/nhess-21-2021-2021>, 2021.

891 Cai, H., Savenije, H. H. G., and Toffolon, M.: Linking the river to the estuary: influence of river discharge on tidal damping,
892 Hydrol. Earth Syst. Sci., 18, 287–304, <https://doi.org/10.5194/hess-18-287-2014>, 2014.

893 Census: Coastal towns in England and Wales: October 2020:
894 <https://www.ons.gov.uk/businessindustryandtrade/tourismindustry/articles/coastaltownsinenglandandwales/2020-10-06>, last
895 access: May 2023, 2020.

896 [Cesbron, G., Melet, A., Almar, R., Lifermann, A., Tullo, D., Crosnier, L.: Pan-European Satellite-Derived Coastal
897 Bathymetry—Review, User Needs and Future Services. Frontiers in Marine Science, 8,
898 <https://doi.org/10.3389/fmars.2021.740830>, 2021.](https://doi.org/10.3389/fmars.2021.740830)

899 Chilton, D., Hamilton, D. P., Nagelkerken, I., Cook, P., Hipsey, M. R., Reid, R., Sheaves, M., Waltham, N. J., and Brookes,
900 J.: Environmental Flow Requirements of Estuaries: Providing Resilience to Current and Future Climate and Direct
901 Anthropogenic Changes, Front. Environ. Sci., 9, <https://doi.org/10.3389/fenvs.2021.764218>, 2021.

902 [Chow, V.T., Maidment, D.R. and Mays, L.W. \(1988\) Applied Hydrology. International Edition, McGraw-Hill Book Company,
903 New York.](https://doi.org/10.1002/9781118409523.ch1)

904 [Cipollini, P., Calafat, F.M., Jevrejeva, S., Melet, A., Prandi, P.: Monitoring Sea Level in the Coastal Zone with Satellite
905 Altimetry and Tide Gauges. Surveys in Geophysics, 38\(1\), 33–57, <https://doi.org/10.1007/s10712-016-9392-0>, 2016.](https://doi.org/10.1007/s10712-016-9392-0)

906 Coles, S.: An Introduction to Statistical Modeling of Extreme Values. Springer, London. [https://doi.org/10.1007/978-1-4471-](https://doi.org/10.1007/978-1-4471-3675-0)
907 [3675-0](https://doi.org/10.1007/978-1-4471-3675-0), 2001.

908 [Costa, W. L. L., Bryan, K. R., and Coco, G.: Modelling extreme water levels using intertidal topography and bathymetry](#)
909 [derived from multispectral satellite images, Nat. Hazards Earth Syst. Sci., 23, 3125–3146, \[https://doi.org/10.5194/nhess-23-\]\(https://doi.org/10.5194/nhess-23-3125-2023\)](#)
910 [3125-2023, 2023.](#)

911 Couasnon, A., Eilander, D., Muis, S., Veldkamp, T. I. E., Haigh, I. D., Wahl, T., Winsemius, H. C., and Ward, P. J.: Measuring
912 compound flood potential from river discharge and storm surge extremes at the global scale, Nat. Hazards Earth Syst. Sci., 20,
913 489–504, <https://doi.org/10.5194/nhess-20-489-2020>, 2020.

914 Coulthard, T. J., Neal, J. C., Bates, P. D., Ramirez, J., de Almeida, G. A. M., and Hancock, G. R.: Integrating the LISFLOOD-
915 FP 2D hydrodynamic model with the CAESAR model: implications for modelling landscape evolution, Earth Surf Processes
916 Landf, 38, 1897–1906, <https://doi.org/10.1002/esp.3478>, 2013.

917 Cutter, S. L., Emrich, C. T., Morath, D. P., and Dunning, C. M.: Integrating social vulnerability into federal flood risk
918 management planning, J Flood Risk Management, 6, 332–344, <https://doi.org/10.1111/jfr3.12018>, 2013.

919 Defra: Flood and coastal erosion risk management Policy Statement:[https://www.gov.uk/government/publications/flood-and-](https://www.gov.uk/government/publications/flood-and-coastal-erosion-risk-management-policy-statement)
920 [coastal-erosion-risk-management-policy-statement](https://www.gov.uk/government/publications/flood-and-coastal-erosion-risk-management-policy-statement), last access: November 2021.

921 Environment Agency: Reliability in Flood Incident Management Planning Final Report – Part A: Guidance Science project
922 SC060063/SR1:
923 https://assets.publishing.service.gov.uk/media/602e8e04d3bf7f722294d1d1/Reliability_in_Flood_Incident_Management_guidance.pdf, last access: November 2021, 2009.

925 Environment Agency: National flood and coastal erosion risk management strategy for England: executive summary:
926 [https://www.gov.uk/government/publications/national-flood-and-coastal-erosion-risk-management-strategy-for-england-](https://www.gov.uk/government/publications/national-flood-and-coastal-erosion-risk-management-strategy-for-england-2/national-flood-and-coastal-erosion-risk-management-strategy-for-england-executive-summary)
927 [2/national-flood-and-coastal-erosion-risk-management-strategy-for-england-executive-summary](https://www.gov.uk/government/publications/national-flood-and-coastal-erosion-risk-management-strategy-for-england-2/national-flood-and-coastal-erosion-risk-management-strategy-for-england-executive-summary), last access: November
928 2021, 2020.

929 Environment Agency: State of the environment: the coastal and marine environment:
930 [https://assets.publishing.service.gov.uk/government/uploads/system/uploads/attachment_data/file/1130743/State_of_the_env](https://assets.publishing.service.gov.uk/government/uploads/system/uploads/attachment_data/file/1130743/State_of_the_environment_-_the_coastal_and_marine_environment_-_report.pdf)
931 [ironment - the coastal and marine environment - report.pdf](https://assets.publishing.service.gov.uk/government/uploads/system/uploads/attachment_data/file/1130743/State_of_the_environment_-_the_coastal_and_marine_environment_-_report.pdf), last access: January 2023.

932 Eichertopf, S., Karunarathna, H., and Alsina, J. M.: Morphodynamics of sandy beaches under the influence of storm
933 sequences: Current research status and future needs, Water Science and Engineering, 12, 221–234,
934 <https://doi.org/10.1016/j.wse.2019.09.007>, 2019.

935 Eilander, D., Couasnon, A., Leijnse, T., Ikeuchi, H., Yamazaki, D., Muis, S., Dullaart, J., Haag, A., Winsemius, H. C., and
936 Ward, P. J.: A globally applicable framework for compound flood hazard modeling, Nat. Hazards Earth Syst. Sci., 23, 823–
937 846, <https://doi.org/10.5194/nhess-23-823-2023>, 2023.

938 Elliott, L. R., White, M. P., Grellier, J., Rees, S. E., Waters, R. D., and Fleming, L. E.: Recreational visits to marine and coastal
939 environments in England: Where, what, who, why, and when?, Marine Policy, 97, 305–314,
940 <https://doi.org/10.1016/j.marpol.2018.03.013>, 2018.

941 Evans, O.: Storm Ciara: Llanrwst, Colwyn Bay and Llanfair TH hit by flooding as torrential rain causes chaos across Conwy:
942 <https://www.dailypost.co.uk/news/north-wales-news/storm-ciara-flooding-hits-communities-17715701>, last access: April
943 2023

- 944 Familkhalili, R., Talke, S. A., and Jay, D. A.: Compound flooding in convergent estuaries: insights from an analytical model,
945 *Ocean Sci.*, 18, 1203–1220, <https://doi.org/10.5194/os-18-1203-2022>, 2022.
- 946 Fekete, A., Aslam, A. B., de Brito, M. M., Dominguez, I., Fernando, N., Illing, C. J., KC, A. K., Mahdavian, F., Norf, C., Platt,
947 S., Santi, P. A., and Tempels, B.: Increasing flood risk awareness and warning readiness by participation – But who understands
948 what under ‘participation’?, *International Journal of Disaster Risk Reduction*, 57, 102157,
949 <https://doi.org/10.1016/j.ijdr.2021.102157>, 2021.
- 950 [Feng, D., Tan, Z., Engwirda, D., Liao, C., Xu, D., Bisht, G., Zhou, T., Li, H.-Y., and Leung, L. R.: Investigating coastal](#)
951 [backwater effects and flooding in the coastal zone using a global river transport model on an unstructured mesh, *Hydrol. Earth*](#)
952 [*Syst. Sci.*, 26, 5473–5491, <https://doi.org/10.5194/hess-26-5473-2022>, 2022.](#)
- 953 Feng, D., Tan, Z., Xu, D., and Leung, L. R.: Understanding the compound flood risk along the coast of the contiguous United
954 States, *Hydrol. Earth Syst. Sci.*, 27, 3911–3934, <https://doi.org/10.5194/hess-27-3911-2023>, 2023. Ferranti, E., Chapman, L.,
955 and Whyatt, D.: A Perfect Storm? The collapse of Lancaster’s critical infrastructure networks following intense rainfall on 4/5
956 December 2015, *Weather*, 72, 3–7, <https://doi.org/10.1002/wea.2907>, 2017.
- 957 FloodList: UK – Flood Rescues After Rivers Overflow in England and Wales: <https://floodlist.com/europe/uk/>
958 [kingdom/rivers-overflow-england-wales-march-2019](#), last access: April 2023.
- 959 Ganguli, P. and Merz, B.: Extreme Coastal Water Levels Exacerbate Fluvial Flood Hazards in Northwestern Europe, *Sci Rep*,
960 9, <https://doi.org/10.1038/s41598-019-49822-6>, 2019.
- 961 Genest, C. and Favre, A.-C.: Everything You Always Wanted to Know about Copula Modeling but Were Afraid to Ask, *J.*
962 *Hydrol. Eng.*, 12, 347–368, [https://doi.org/10.1061/\(asce\)1084-0699\(2007\)12:4\(347\)](https://doi.org/10.1061/(asce)1084-0699(2007)12:4(347)), 2007.
- 963 Ghanbari, M., Arabi, M., Kao, S., Obeysekera, J., and Sweet, W.: Climate Change and Changes in Compound Coastal-Riverine
964 Flooding Hazard Along the U.S. Coasts, *Earth’s Future*, 9, <https://doi.org/10.1029/2021ef002055>, 2021.
- 965 Gori, A. and Lin, N.: Projecting Compound Flood Hazard Under Climate Change With Physical Models and Joint Probability
966 Methods, *Earth’s Future*, 10, <https://doi.org/10.1029/2022ef003097>, 2022.
- 967 Greenwood, C. and Nikulin, M.S.: A guide to chi-squared testing, Wiley. New York [ISBN 0-471-55779-X](#), 1996.
- 968 Gupta, H. V., Kling, H., Yilmaz, K. K., and Martinez, G. F.: Decomposition of the mean squared error and NSE performance
969 criteria: Implications for improving hydrological modelling, *Journal of Hydrology*, 377, 80–91,
970 <https://doi.org/10.1016/j.jhydrol.2009.08.003>, 2009.
- 971 The First Global Integrated Marine Assessment, Cambridge University Press, <https://doi.org/10.1017/9781108186148>, 2017.
- 972 Haigh, I. D., Wadey, M. P., Gallop, S. L., Loehr, H., Nicholls, R. J., Horsburgh, K., Brown, J. M., and Bradshaw, E.: A user-
973 friendly database of coastal flooding in the United Kingdom from 1915–2014, *Sci Data*, 2,
974 <https://doi.org/10.1038/sdata.2015.21>, 2015.
- 975 Haigh, I. D., Wadey, M. P., Wahl, T., Ozsoy, O., Nicholls, R. J., Brown, J. M., Horsburgh, K., and Gouldby, B.: Spatial and
976 temporal analysis of extreme sea level and storm surge events around the coastline of the UK, *Sci Data*, 3,
977 <https://doi.org/10.1038/sdata.2016.107>, 2016.
- 978 Haigh, I. D., Ozsoy, O., Wadey, M. P., Nicholls, R. J., Gallop, S. L., Wahl, T., and Brown, J. M.: An improved database of
979 coastal flooding in the United Kingdom from 1915 to 2016, *Sci Data*, 4, <https://doi.org/10.1038/sdata.2017.100>, 2017.

980 [Harrigan, S., Zsoter, E., Alfieri, L., Prudhomme, C., Salamon, P., Wetterhall, F., Barnard, C., Cloke, H., Pappenberger, F.:](#)
981 [GloFAS-ERA5 operational global river discharge reanalysis 1979–present.](#) *Earth System Science Data*. 12(3), 2043–2060,
982 <https://doi.org/10.5194/essd-12-2043-2020>, 2020.

983 Harrison, L. M., Coulthard, T. J., Robins, P. E., and Lewis, M. J.: Sensitivity of Estuaries to Compound Flooding, *Estuaries*
984 *and Coasts*, 45, 1250–1269, <https://doi.org/10.1007/s12237-021-00996-1>, 2021.

985 [Hasan, G.M.J., Matin, N.: Intertidal bathymetry and foreshore slopes derived from satellite images for static coasts.](#) *Regional*
986 *Studies in Marine Science*. 51, 102233, <https://doi.org/10.1016/j.rsma.2022.102233>, 2022.

987 Heimhuber, V., Vos, K., Fu, W., Glamore, W.: InletTracker: An open- source Python toolkit for historic and near real-time
988 monitoring of coastal inlets from Landsat and Sentinel-2, *Geomorphology*, 389,
989 <https://doi.org/10.1016/j.geomorph.2021.107830>, 2021.

990 Hendry, A., Haigh, I. D., Nicholls, R. J., Winter, H., Neal, R., Wahl, T., Joly-Laugel, A., and Darby, S. E.: Assessing the
991 characteristics and drivers of compound flooding events around the UK coast, *Hydrol. Earth Syst. Sci.*, 23, 3117–3139,
992 <https://doi.org/10.5194/hess-23-3117-2019>, 2019.

993 Hoitink, A. J. F. and Jay, D. A.: Tidal river dynamics: Implications for deltas, *Reviews of Geophysics*, 54, 240–272,
994 <https://doi.org/10.1002/2015rg000507>, 2016.

995 [Holgate, S.J., Matthews, A., Woodworth, P.L., Rickards, L.J., Tamisiea, M.E., Bradshaw, E., Foden, P.R., Gordon, K.M.,](#)
996 [Jevrejeva, S., Pugh, J.: New Data Systems and Products at the Permanent Service for Mean Sea Level.](#) *Journal of Coastal*
997 *Research*. 29(3), 493, <https://doi.org/10.2112/JCOASTRES-D-12-00175.1>, 2013.

998 Howlett, E. R., Bowers, D. G., Malarkey, J., and Jago, C. F.: Stratification in the presence of an axial convergent front: Causes
999 and implications, *Estuarine, Coastal and Shelf Science*, 161, 1–10, <https://doi.org/10.1016/j.ecss.2015.04.003>, 2015.

1000 HR Wallingford: Conwy Tidal Flood Risk Assessment:
1001 http://conwyfloodmap.hrwallingford.co.uk/report/HRWallingford_ConwyFRA_Stage1_Report_EX4667.pdf, last access:
1002 April 2023, 2008.

1003 [IHO C-55: Publication C-55 “Status of Hydrographic Surveying and Charting Worldwide.”.](#) Monte Carlo: IHO,
1004 <https://iho.int/en/iho-c-55>, 2021.

1005 [Ikeuchi, H., Hirabayashi, Y., Yamazaki, D., Kiguchi, M., Koirala, S., Nagano, T., Kotera, A., Kanae, S.: Modeling complex](#)
1006 [flow dynamics of fluvial floods exacerbated by sea level rise in the Ganges–Brahmaputra–Meghna Delta.](#) *Environ. Res. Lett.*
1007 *10* 124011, <https://doi.org/10.1088/1748-9326/10/12/124011>, 2015.

1008 ITV: Flood warnings as downpours and high tides hit Wales: [https://www.itv.com/news/wales/2015-12-26/flood-warnings-at-](https://www.itv.com/news/wales/2015-12-26/flood-warnings-at-downpours-and-high-tides-hit-wales)
1009 [downpours-and-high-tides-hit-wales](https://www.itv.com/news/wales/2015-12-26/flood-warnings-at-downpours-and-high-tides-hit-wales), last access: April 2023, 2015.

1010

1011 [Jago, C., Robins, P., Howlett, E., Hassard, F., Raiko-Nenow, P., Jackson, S., Chien, N., & Malham, S.: Trapping and](#)
1012 [bypassing of suspended particulate matter, particulate nutrients and faecal indicator organisms in the River-Estuary transition](#)
1013 [zone of a shallow Macrotidal Estuary.](#) *Science of The Total Environment* (in review).

1014 Jones, M.: Boxing Day floods 2015: How North Wales ground to a halt during the deluge:
1015 <https://www.dailypost.co.uk/news/north-wales-news/boxing-day-floods-2015-how-12370017>, last access: May 2023, 2015.

- 1016 Juárez, B., Stockton, S. A., Serafin, K. A., and Valle-Levinson, A.: Compound Flooding in a Subtropical Estuary Caused by
1017 Hurricane Irma 2017, *Geophysical Research Letters*, 49, <https://doi.org/10.1029/2022gl099360>, 2022.
- 1018 Khajehei, S., Ahmadi, A., and Moradkhani, H.: An effective post-processing of the North American multi-model
1019 ensemble (NMME) precipitation forecasts over the continental US, *Clim Dyn*, 51, 457–472, [https://doi.org/10.1007/s00382-](https://doi.org/10.1007/s00382-017-3934-0)
1020 017-3934-0, 2017.
- 1021 Khanam, M., Sofia, G., Koukoulou, M., Lazin, R., Nikolopoulos, E. I., Shen, X., and Anagnostou, E. N.: Impact of compound
1022 flood event on coastal critical infrastructures considering current and future climate, *Nat. Hazards Earth Syst. Sci.*, 21, 587–
1023 605, <https://doi.org/10.5194/nhess-21-587-2021>, 2021.
- 1024 [Khojasteh, D., Glamore, W., Heimhuber, V., and Felder, S. Sea level rise impacts on estuarine dynamics: A review. *Science of the Total Environment*, 780, <https://doi.org/10.1016/j.scitotenv.2021.146470>, 2021.](#)
- 1025
- 1026 [Lavers, D., Harrigan, S., Andersson, E., Richardson, D. S., Prudhomme, C., and Pappenberger, F.: A vision for improving global flood forecasting. *Environ. Res. Lett.*, 14, 121002, <https://doi.org/10.1088/1748-9326/ab52b2>, 2019.](#)
- 1027
- 1028 Lane, R. A., Coxon, G., Freer, J., Seibert, J., and Wagener, T.: A large-sample investigation into uncertain climate change
1029 impacts on high flows across Great Britain, *Hydrol. Earth Syst. Sci.*, 26, 5535–5554, [https://doi.org/10.5194/hess-26-5535-](https://doi.org/10.5194/hess-26-5535-2022)
1030 2022, 2022.
- 1031 Lindeboom, H. The Coastal Zone: An Ecosystem Under Pressure. In *Oceans 2020: Science, Trends and the Challenge of*
1032 *Sustainability*; Field, J.G., Hempel, G., Summerhayes, C.P., Eds.; Island Press: Washington, DC, USA; pp. 49–84. ISBN 1-
1033 55963-470-7, 2002
- 1034 Lyddon, C., Brown, J. M., Leonardi, N., and Plater, A. J.: Flood Hazard Assessment for a Hyper-Tidal Estuary as a Function
1035 of Tide-Surge-Morphology Interaction, *Estuaries and Coasts*, 41, 1565–1586, <https://doi.org/10.1007/s12237-018-0384-9>,
1036 2018.
- 1037 Lyddon, C. E., Brown, J. M., Leonardi, N., Saulter, A., and Plater, A. J.: Quantification of the Uncertainty in Coastal Storm
1038 Hazard Predictions Due to Wave-Current Interaction and Wind Forcing, *Geophysical Research Letters*, 46, 14576–14585,
1039 <https://doi.org/10.1029/2019gl086123>, 2019.
- 1040 Lyddon, C., Robins, P., Lewis, M., Barkwith, A., Vasilopoulos, G., Haigh, I., and Coulthard, T.: Historic Spatial Patterns of
1041 Storm-Driven Compound Events in UK Estuaries, *Estuaries and Coasts*, 46, 30–56, [https://doi.org/10.1007/s12237-022-](https://doi.org/10.1007/s12237-022-01115-4)
1042 01115-4, 2022.
- 1043 [Marcos, M., Wöppelmann, G., Matthews, A., Ponte, R.M., Birol, F., Arduin, F., Coco, G., Santamaría-Gómez, A., Ballu, V., Testut, L., Chambers, D., Stopa, J.E.: Coastal Sea Level and Related Fields from Existing Observing Systems. *Surveys in Geophysics*. 40\(6\), 1293–1317, <https://doi.org/10.1007/s10712-019-09513-3>, 2019.](#)
- 1044
- 1045
- 1046 Matthews, T., Murphy, C., McCarthy, G., Broderick, C., and Wilby, R. L.: Super Storm Desmond: a process-based assessment,
1047 *Environ. Res. Lett.*, 13, 014024, <https://doi.org/10.1088/1748-9326/aa98c8>, 2018.
- 1048 Met Office: Stormy and very wet spell March 2019:
1049 [https://www.metoffice.gov.uk/binaries/content/assets/metofficegovuk/pdf/weather/learn-about/uk-past-](https://www.metoffice.gov.uk/binaries/content/assets/metofficegovuk/pdf/weather/learn-about/uk-past-events/interesting/2019/2019_004_stormy_spell.pdf)
1050 [events/interesting/2019/2019_004_stormy_spell.pdf](https://www.metoffice.gov.uk/binaries/content/assets/metofficegovuk/pdf/weather/learn-about/uk-past-events/interesting/2019/2019_004_stormy_spell.pdf) last access: May 2023, 2019.
- 1051 Moftakhari, H. R., Salvadori, G., AghaKouchak, A., Sanders, B. F., and Matthew, R. A.: Compounding effects of sea level
1052 rise and fluvial flooding, *Proc. Natl. Acad. Sci. U.S.A.*, 114, 9785–9790, <https://doi.org/10.1073/pnas.1620325114>, 2017.

1053 Moore, F. C. and Obradovich, N.: Using remarkability to define coastal flooding thresholds, *Nat Commun*, 11,
1054 <https://doi.org/10.1038/s41467-019-13935-3>, 2020.

1055 Moradian, S., Olbert, A. I., Gharbia, S., and Iglesias, G.: Copula-based projections of wind power: Ireland as a case study,
1056 *Renewable and Sustainable Energy Reviews*, 175, 113147, <https://doi.org/10.1016/j.rser.2023.113147>, 2023.

1057 Muis, S., Verlaan, M., Winsemius, H. C., Aerts, J. C. J. H., and Ward, P. J.: A global reanalysis of storm surges and extreme
1058 sea levels, *Nat Commun*, 7, <https://doi.org/10.1038/ncomms11969>, 2016.

1059 Muis, S., Apecechea, M. I., Dullaart, J., de Lima Rego, J., Madsen, K. S., Su, J., Yan, K., and Verlaan, M.: A High-Resolution
1060 Global Dataset of Extreme Sea Levels, Tides, and Storm Surges, Including Future Projections, *Front. Mar. Sci.*, 7,
1061 <https://doi.org/10.3389/fmars.2020.00263>, 2020.

1062 [Muis, S., Aerts, J.C.J.H., Á. Antolínez, J.A., Dullaart, J.C., Duong, T.M., Erikson, L., Haarsma, R.J., Apecechea, M.I., Mengel,
1063 M., Le Bars, D., O'Neill, A., Ranasinghe, R., Roberts, M.J., Verlaan, M., Ward, P.J., Yan, K. \(2023\) Global Projections of
1064 Storm Surges Using High-Resolution CMIP6 Climate Models. *Earth's Future*. 11\(9\). <https://doi.org/10.1029/2023EF003479>,
1065 2023.](https://doi.org/10.1029/2023EF003479)

1066 Nasr, A. A., Wahl, T., Rashid, M. M., Camus, P., and Haigh, I. D.: Assessing the dependence structure between oceanographic,
1067 fluvial, and pluvial flooding drivers along the United States coastline, *Hydrol. Earth Syst. Sci.*, 25, 6203–6222,
1068 <https://doi.org/10.5194/hess-25-6203-2021>, 2021.

1069 Natural Resource Wales Flood Investigation Report: Llanrwst Flooding December 2015 [online] Available at:
1070 <https://naturalresources.wales/media/678788/flood-investigation-report-llanrwst-2015-english.pdf> last access: November
1071 2022, 2016.

1072 Natural Resource Wales: DataMap Wales: Recorded Flood Extents (Formerly Lle): [https://datamap.gov.wales/layers/inspire-
1073 nrw:NRW_HISTORIC_FLOODMAP#/](https://datamap.gov.wales/layers/inspire-nrw:NRW_HISTORIC_FLOODMAP#/) last access: November 2022, 2020.

1074 Natural Resource Wales: Historic Flood Map: [https://datamap.gov.wales/maps/new?layer=inspire-
1075 nrw:NRW_HISTORIC_FLOODMAP#/](https://datamap.gov.wales/maps/new?layer=inspire-nrw:NRW_HISTORIC_FLOODMAP#/) last access: January 2023.

1076 National Coastal Tourism Academy: Coastal Tourism: <https://coastaltourismacademy.co.uk/coastal-tourism> last access:
1077 August 2023.

1078 Neal, J., Hawker, L., Savage, J., Durand, M., Bates, P., and Sampson, C.: Estimating River Channel Bathymetry in Large Scale
1079 Flood Inundation Models, *Water Resources Research*, 57, <https://doi.org/10.1029/2020wr028301>, 2021.

1080 Nelsen, Roger B.: An introduction to Copulas. Springer Series in Statistics. Second edition. Department of Mathematical
1081 Sciences. Lewis & Clark College, MSC 110, ISBN 978-0-387-28678-5, 2007.

1082 O'Donnell, E. C. and Thorne, C. R.: Drivers of future urban flood risk, *Phil. Trans. R. Soc. A.*, 378, 20190216,
1083 <https://doi.org/10.1098/rsta.2019.0216>, 2020.

1084 Olbert, A. I., Moradian, S., Nash, S., Comer, J., Kazmierczak, B., Falconer, R. A., and Hartnett, M.: Combined statistical and
1085 hydrodynamic modelling of compound flooding in coastal areas - Methodology and application, *Journal of Hydrology*, 620,
1086 129383, <https://doi.org/10.1016/j.jhydrol.2023.129383>, 2023.

1087 ONR: ONR Expert Panel on Natural Hazards, Analysis of Coastal Flood Hazards for Nuclear Sites: 2021
1088 https://www.onr.org.uk/operational/tech_asst_guides/ns-tast-gd-013-annex-3-reference-paper.docx. Last access: October
1089 2023, 2021.

1090 Pawłowicz, R., Beardsley, B., and Lentz, S.: Classical tidal harmonic analysis including error estimates in MATLAB using
1091 T_TIDE, *Computers & Geosciences*, 28, 929–937, [https://doi.org/10.1016/s0098-3004\(02\)00013-4](https://doi.org/10.1016/s0098-3004(02)00013-4), 2002.

1092 Peter Sheng, Y., Paramygin, V. A., Yang, K., and Rivera-Nieves, A. A.: A sensitivity study of rising compound coastal
1093 inundation over large flood plains in a changing climate, *Sci Rep*, 12, <https://doi.org/10.1038/s41598-022-07010-z>, 2022.

1094 Penning-Rowsell, E. C.: A realistic assessment of fluvial and coastal flood risk in England and Wales, *Trans Inst British Geog*,
1095 40, 44–61, <https://doi.org/10.1111/tran.12053>, 2014.

1096 [Pugh, D.T. Tides, surges and mean sea-level \(reprinted with corrections\), Chichester, UK. John Wiley & Sons, Ltd, 1996.](#)

1097 Rahimi, R., Tavakol-Davani, H., Graves, C., Gomez, A., and Fazel Valipour, M.: Compound Inundation Impacts of Coastal
1098 Climate Change: Sea-Level Rise, Groundwater Rise, and Coastal Precipitation, *Water*, 12, 2776,
1099 <https://doi.org/10.3390/w12102776>, 2020.

1100 Rilo, A., Tavares, A. O., Freire, P., Zêzere, J. L., and Haigh, I. D.: Improving Estuarine Flood Risk Knowledge through
1101 Documentary Data Using Multiple Correspondence Analysis, *Water*, 14, 3161, <https://doi.org/10.3390/w14193161>, 2022.

1102 [Robins, P. E., Neill, S. P., and Giménez, L.: A numerical study of marine larval dispersal in the presence of an axial convergent
1103 front, *Estuarine, Coastal and Shelf Science*, 100, 172–185, <https://doi.org/10.1016/j.ecss.2012.02.001>, 2012.](#)

1104 Robins, P. E., Skov, M. W., Lewis, M. J., Giménez, L., Davies, A. G., Malham, S. K., Neill, S. P., McDonald, J. E., Whitton,
1105 T. A., Jackson, S. E., and Jago, C. F.: Impact of climate change on UK estuaries: A review of past trends and potential
1106 projections, *Estuarine, Coastal and Shelf Science*, 169, 119–135, <https://doi.org/10.1016/j.ecss.2015.12.016>, 2016.

1107 Robins, P. E., Lewis, M. J., Elnahrawi, M., Lyddon, C., Dickson, N., and Coulthard, T. J.: Compound Flooding: Dependence
1108 at Sub-daily Scales Between Extreme Storm Surge and Fluvial Flow, *Front. Built Environ.*, 7,
1109 <https://doi.org/10.3389/fbuil.2021.727294>, 2021.

1110 Sadegh, M., Ragno, E., and AghaKouchak, A.: Multivariate Copula Analysis Toolbox (MvCAT): Describing dependence and
1111 underlying uncertainty using a Bayesian framework, *Water Resources Research*, 53, 5166–5183,
1112 <https://doi.org/10.1002/2016wr020242>, 2017.

1113 Sadegh, M., Moftakhari, H., Gupta, H. V., Ragno, E., Mazdiyasi, O., Sanders, B., Matthew, R., and AghaKouchak, A.:
1114 Multihazard Scenarios for Analysis of Compound Extreme Events, *Geophysical Research Letters*, 45, 5470–5480,
1115 <https://doi.org/10.1029/2018gl077317>, 2018.

1116 Šakić Trogrlić, R., van den Homberg, M., Budimir, M., McQuistan, C., Sneddon, A., and Golding, B.: Early Warning Systems
1117 and Their Role in Disaster Risk Reduction, Towards the “Perfect” Weather Warning, 11–46, https://doi.org/10.1007/978-3-030-98989-7_2, 2022.

1119 Sene, K.: Thresholds. In: *Flood Warning, Forecasting and Emergency Response*. Springer, Berlin, Heidelberg.
1120 https://doi.org/10.1007/978-3-540-77853-0_3, 2008.

- 1121 Skinner, C. J., Coulthard, T. J., Parsons, D. R., Ramirez, J. A., Mullen, L., and Manson, S.: Simulating tidal and storm surge
1122 hydraulics with a simple 2D inertia based model, in the Humber Estuary, U.K, *Estuarine, Coastal and Shelf Science*, 155, 126–
1123 136, <https://doi.org/10.1016/j.ecss.2015.01.019>, 2015.
- 1124 Sklar.: Fonctions de répartition à n dimensions et leurs marges. *Publications de l'Institut de Statistique de l'Université de Paris*,
1125 8, 229–231, 1959.
- 1126 Sibley, A., Cox, D., and Titley, H.: Coastal flooding in England and Wales from Atlantic and North Sea storms during the
1127 2013/2014 winter, *Weather*, 70, 62–70, <https://doi.org/10.1002/wea.2471>, 2015.
- 1128 Spridgeon, D.: Aberconwy AM to ask emergency questions over Conwy Valley flooding:
1129 <https://www.northwalespioneer.co.uk/news/18222471.aberconwy-ask-emergency-questions-conwy-valley-flooding/> last
1130 access: April 2023, 2020.
- 1131 Svensson, C. and Jones, D. A.: Dependence between sea surge, river flow and precipitation in south and west Britain, *Hydrol.*
1132 *Earth Syst. Sci.*, 8, 973–992, <https://doi.org/10.5194/hess-8-973-2004>, 2004.
- 1133 [Vasilopoulos, G., Coulthard, T., Robins, P., Lyddon, C., Barkwith, A., Chien, N., and Lewis, M.: Development and validation
1134 of flood inundation models for estuaries, EGU General Assembly 2023, Vienna, Austria, 23–28 Apr 2023, EGU23-5858,
1135 <https://doi.org/10.5194/egusphere-egu23-5858>, 2023.](https://doi.org/10.5194/egusphere-egu23-5858)
- 1136 Wang, X., Verlaan, M., Apecechea, M. I., and Lin, H. X.: Parameter estimation for a global tide and surge model with a
1137 memory-efficient order reduction approach, *Ocean Modelling*, 173, 102011, <https://doi.org/10.1016/j.ocemod.2022.102011>,
1138 2022.
- 1139 Ward, P. J., Couason, A., Eilander, D., Haigh, I. D., Hendry, A., Muis, S., Veldkamp, T. I. E., Winsemius, H. C., and Wahl,
1140 T.: Dependence between high sea-level and high river discharge increases flood hazard in global deltas and estuaries, *Environ.*
1141 *Res. Lett.*, 13, 084012, <https://doi.org/10.1088/1748-9326/aad400>, 2018.
- 1142 Welsh Government (2015) CABINET STATEMENT Coastal flooding – January 2014: [https://www.gov.wales/written-
1143 statement-coastal-flooding-january-2014](https://www.gov.wales/written-statement-coastal-flooding-january-2014) last access: April 2023, 2014.
- 1144 Welsh Government (2015) CABINET STATEMENT Flooding in North Wales December 2015:
1145 <https://www.gov.wales/written-statement-flooding-north-wales-december-2015> last access: April 2023, 2015.
- 1146 Wolff, E.: The promise of a “people-centred” approach to floods: Types of participation in the global literature of citizen
1147 science and community-based flood risk reduction in the context of the Sendai Framework, *Progress in Disaster Science*, 10,
1148 100171, <https://doi.org/10.1016/j.pdisas.2021.100171>, 2021.
- 1149 [Wu, W., Westra, S., Leonard, M.: Estimating the probability of compound floods in estuarine regions. *Hydrology and Earth
1150 System Sciences*. 25\(5\), 2821–2841, 2021.](https://doi.org/10.1016/j.jhydrol.2021.2821-2841)
- 1151 Xiao, Z., Yang, Z., Wang, T., Sun, N., Wigmosta, M., and Judi, D.: Characterizing the Non-linear Interactions Between Tide,
1152 Storm Surge, and River Flow in the Delaware Bay Estuary, United States, *Front. Mar. Sci.*, 8,
1153 <https://doi.org/10.3389/fmars.2021.715557>, 2021.
- 1154 Yagoub, M. M., Alseireidi, A. A., Mohamed, E. A., Periyasamy, P., Alameri, R., Aldarmaki, S., and Alhashmi, Y.: Newspapers
1155 as a validation proxy for GIS modeling in Fujairah, United Arab Emirates: identifying flood-prone areas, *Nat Hazards*, 104,
1156 111–141, <https://doi.org/10.1007/s11069-020-04161-y>, 2020.

1157 Yazdandoost, F., Moradian, S., Zakipour, M., Izadi, A., and Bavandpour, M.: Improving the precipitation forecasts of the
1158 North-American multi model ensemble (NMME) over Sistan basin, *Journal of Hydrology*, 590, 125263,
1159 <https://doi.org/10.1016/j.jhydrol.2020.125263>, 2020.

1160 Zscheischler, J., Westra, S., van den Hurk, B. J. J. M., Seneviratne, S. I., Ward, P. J., Pitman, A., AghaKouchak, A., Bresch,
1161 D. N., Leonard, M., Wahl, T., and Zhang, X.: Future climate risk from compound events, *Nature Clim Change*, 8, 469–477,
1162 <https://doi.org/10.1038/s41558-018-0156-3>, 2018.

1163 Zong, Y., Tooley, M.J. A.: Historical Record of Coastal Floods in Britain: Frequencies and Associated Storm Tracks. *Natural*
1164 *Hazards* 29, 13–36, <https://doi.org/10.1023/A:1022942801531>

1165